

1 Observations of particle number size distributions and new 2 particle formation in six Indian locations

3
4 Mathew Sebastian¹, Sobhan Kumar Kompalli², Vasudevan Anil Kumar³, Sandhya Jose^{4,5}, S.
5 Suresh Babu², Govindan Pandithurai³, Sachchidanand Singh^{4,5}, Rakesh K. Hooda⁶, Vijay K. Soni⁷,
6 Jeffrey R. Pierce⁸, Ville Vakkari^{6,9}, Eija Asmi⁶, Daniel M. Westervelt^{10,11}, Antti-P. Hyvärinen⁶,
7 and Vijay P. Kanawade^{1,*}

8
9 ¹Centre for Earth, Ocean and Atmospheric Sciences, University of Hyderabad, Hyderabad, India

10 ²Space Physics Laboratory, Vikram Sarabhai Space Centre, Thiruvananthapuram, India

11 ³Indian Institute of Tropical Meteorology, Ministry of Earth Sciences, Pune, India

12 ⁴CSIR-National Physical Laboratory, Dr. K.S. Krishnan Road, New Delhi, India

13 ⁵Academy of Scientific and Innovative Research (AcSIR), Ghaziabad-201002, India

14 ⁶Finnish Meteorological Institute, Erik Palménin Aukio 1, Helsinki, Finland

15 ⁷India Meteorological Department, Ministry of Earth Sciences, New Delhi, India

16 ⁸Department of Atmospheric Science, Colorado State University, Fort Collins, CO, USA

17 ⁹Atmospheric Chemistry Research Group, Chemical Resource Beneficiation, North-West University, Potchefstroom,
18 South Africa

19 ¹⁰Lamont-Doherty Earth Observatory of Columbia University, New York, USA

20 ¹¹NASA Goddard Institute for Space Studies, New York, NY, USA

21
22 Correspondence to: Vijay P. Kanawade (vijaykanawade03@yahoo.co.in)

23
24 **Abstract.** Atmospheric new particle formation (NPF) is a crucial process driving aerosol number
25 concentrations in the atmosphere; it can significantly impact the evolution of atmospheric aerosol
26 and cloud processes. This study analyses at least one year of asynchronous particle number size
27 distributions from six different locations in India. We also analyze the frequency of NPF and its
28 contribution to cloud condensation nuclei (CCN) concentrations. We found that the NPF frequency
29 has a considerable seasonal variability. At the measurement sites analyzed in this study, NPF
30 frequently occurs in March-May (pre-monsoon, about 21% of the days) and is the least common
31 in October-November (post-monsoon, about 7% of the days). Considering the NPF events in all
32 locations, the particle formation rate (J_{SDS}) varied by more than two orders of magnitude (0.001 -

33 0.6 cm⁻³ s⁻¹) and the growth rate between the smallest detectable size and 25 nm (GR_{sDS-25nm}) by
34 about three orders of magnitude (0.2 - 17.2 nm h⁻¹). We found that J_{sDS} was higher by nearly an
35 order of magnitude during NPF events in urban areas than mountain sites. GR_{sDS} did not show a
36 systematic difference. Our results showed that NPF events could significantly modulate the shape
37 of particle number size distributions and CCN concentrations in India. The contribution of a given
38 NPF event to CCN concentrations was the highest in urban locations (4.3×10³ cm⁻³ per event and
39 1.2×10³ cm⁻³ per event for 50 nm and 100 nm, respectively) as compared to mountain-background
40 sites (2.7×10³ cm⁻³ per event and 1.0×10³ cm⁻³ per event, respectively). We emphasize that the
41 physical and chemical pathways responsible for NPF and factors that control its contribution to
42 CCN production require in-situ field observations using the recent advances in aerosol and its
43 precursor gaseous measurement techniques

44

45 **Keywords:** new particle formation, particle number size distribution, Aitken mode, accumulation
46 mode, cloud condensation nuclei

47

48 **1 Introduction**

49 Cooling by atmospheric aerosols offset a significant fraction of the radiative forcing of the
50 greenhouse gases (Paasonen et al., 2013) directly by scattering and absorbing solar radiation and
51 indirectly by altering cloud microphysical properties via activation of cloud condensation nuclei
52 (CCN) (Rosenfeld et al., 2014; Sarangi et al., 2018). New particle formation (NPF), as a result of
53 the gas-to-particle conversion, is the largest source of the aerosol numbers_s to the terrestrial
54 atmosphere (Kulmala et al., 2007; Zhang et al., 2012). While nucleated particles from NPF are
55 initially very small molecular clusters (1-2 nm; Kerminen et al., 2012), these molecular clusters
56 can grow to large sizes within a few hours to a few days and ultimately reach CCN-active sizes
57 (>50-100 nm) (Pierce and Adams, 2007; Westervelt et al., 2013). Thus, CCN forms the direct
58 microphysical link between aerosols and clouds and plays a vital role in the hydrological cycle and
59 climate.

60 In India, several intensive field campaigns such as the Indian Ocean Experiment
61 (INDOEX) (Ramanathan et al., 2001), Indian Space Research Organization (ISRO)-Geosphere-
62 Biosphere Programme (GBP)- Land campaign II (Tripathi et al., 2006; Tare et al., 2006), and
63 Integrated Campaign for Aerosols, gases, and Radiation Budget (ICARB) (Moorthy et al., 2008;

64 Nair et al., 2020; Kompalli et al., 2020) measured sub-micron particle number size distributions
65 (PNSDs). There are also short- and long-term field observations of sub-micron PNSDs in a variety
66 of diverse locations in India (Hyvärinen et al., 2010; Kanawade et al., 2014a; Shika et al., 2020;
67 Tripathi et al., 1988; Komppula et al., 2009; Singh et al., 2004; Moorthy et al., 2011; Babu et al.,
68 2016; Kompalli et al., 2018). But there are sparse studies in India characterizing seasonal variation
69 in PNSDs and number concentrations (Kanawade et al., 2014a; Hyvärinen et al., 2010; Komppula
70 et al., 2009; Hooda et al., 2018; Laj et al., 2020) and atmospheric NPF (Sebastian et al., 2021b;
71 Siingh et al., 2018; Neitola et al., 2011; Moorthy et al., 2011; Kanawade et al., 2014b; Kanawade
72 et al., 2014c; Kanawade et al., 2020a). The characterization of PNSDs is critical because the PNSD
73 is controlled by an evolving balance between NPF, condensation of vapor on pre-existing particles,
74 evaporation of particles, coagulation and sedimentation (Ipcc, 2013). Previous field measurements
75 and modeling studies globally demonstrated a substantial enhancement in CCN number
76 concentrations from nucleation (Yu et al., 2020; Wiedensohler et al., 2009; Sihto et al., 2011; Rose
77 et al., 2017; Tröstl et al., 2016; Kalivitis et al., 2015; Westervelt et al., 2013; Pierce et al., 2012;
78 Pierce et al., 2014; Westervelt et al., 2014; Kerminen et al., 2012; Kerminen et al., 2018; Merikanto
79 et al., 2009; Gordon et al., 2017). For instance, Merikanto et al. (2009) revealed that 45% of the
80 global low-level CCN at 0.2% supersaturation originates from nucleation. Westervelt et al. (2014)
81 also found that nucleation contributes to about half of the boundary layer CCN (at supersaturation
82 of 0.2%), with an estimated uncertainty range of 49 to 78%, which is sensitive to the choice of
83 nucleation scheme. In contrast, Reddington et al. (2011), using the global model GLOMAP against
84 ground-based measurements at 15 European sites, found that CCN-sized particle number
85 concentrations were driven by processes other than nucleation at more than ten sites. They
86 explained that the weakened response of CCN-sized particles to boundary layer nucleation arises
87 from an increase in coagulation and condensation sinks for ultrafine particles, thereby reducing
88 the condensational growth of ultrafine particles to CCN-active sizes (Kuang et al., 2009; Pierce
89 and Adams, 2007). Tröstl et al. (2016) also revealed that only a small fraction of total particles less
90 than 50 nm grew beyond 90 nm (50-100 particles cm^{-3}), even on a timescale of several days.
91 Therefore, to better understand atmospheric NPF and its contribution to the boundary layer CCN
92 budget, we need highly-resolved spatiotemporal observational data in diverse environments
93 globally, aided with aerosol model simulations, to help to interpret field observations.

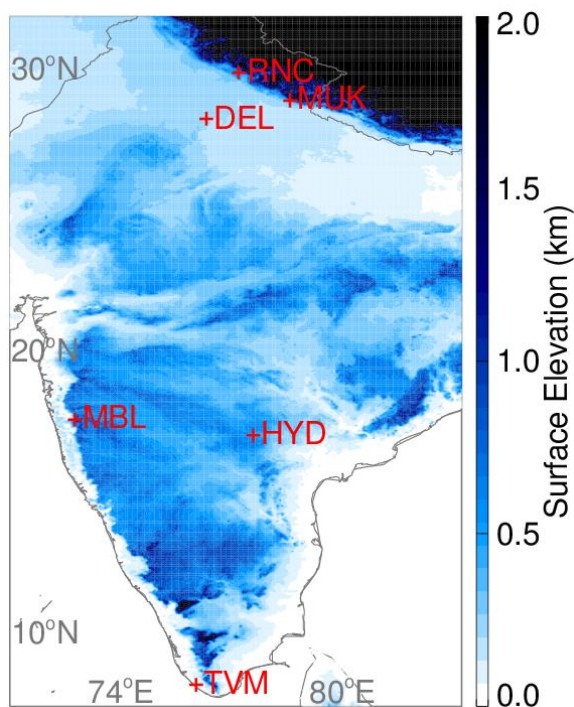
94 Overall, studies pertinent to the impact of NPF on aerosol-cloud interactions are highly
95 sparse in India. The sources of aerosols, and gaseous precursors required for secondary aerosol
96 formation, depict a considerable spatiotemporal heterogeneity over India. Therefore, observational
97 aerosols and precursors data must be synthesized to understand the processes that govern NPF and
98 its contribution to CCN concentrations in different settings of India. The primary objective of this
99 study is to harmonize observational PNSDs data from six diverse locations in India to present
100 analyses of PNSDs, atmospheric NPF, and the contribution of NPF to CCN concentrations.

101

102 2 Methods

103 2.1 Observation sites and aerosol sampling instrumentation

104 Figure 1 shows the geographical location of measurement sites on the surface elevation
105 map. Table 1 provides details of measurement sites and particle data analyzed in this study.



106

107 **Figure 1.** The geographical location of measurement sites on the surface elevation map.
108 Measurement sites such as Ranichauri (RNC), Mukteshwar (MUK), Mahabaleshwar (MBL),
109 Hyderabad (HYD), Thiruvananthapuram (TVM), and Delhi (DEL) are shown by the red plus sign.
110 The global 1-arcsecond (30-m) SRTM digital surface elevation data is obtained from the United
111 States Geological Survey (https://dds.cr.usgs.gov/srtm/version2_1/SRTM30/).

112 **Table 1.** Details of the measurement sites and particle number size distribution measurements
 113 analyzed in this study.

Site Name	Site code	Site type	Instrument	Size range (nm)	Time resolution (minutes)	Time Period
Ranichauri	RNC	Mountain background	DMPS	10.1–757	10	12/2016 – 09/2018
Mukteshwar	MUK	Mountain background	DMPS	10.1–757	5	01/2012 – 12/2013
Mahabaleshwar	MBL	Mountain semi-rural	WRAS	5.14–1000	4	03/2015 – 03/2016
Hyderabad	HYD	Urban	SMPS	10.9–514	5	04/2019 – 03/2020
Thiruvananthapuram	TVM	Semi-urban coastal	SMPS	14.6–661.2	5	01/2013 – 01/2014
Delhi	DEL	Urban	WRAS	5.14–1000	5	11/2011 – 01/2013

114 DMPS: Differential Mobility Particle Sizer, WRAS: Wide-Range Aerosol Spectrometer, SMPS:
 115 Scanning Mobility Particle Sizer

116
 117 Ranichauri observation site (RNC, 30.2° N, 78.25° E; ~1930 m above mean sea level, amsl)
 118 is located in Tehri–Garhwal district of Uttarakhand state in the southern slope of the Western
 119 Himalaya. The RNC site is situated on an isolated hilltop within the campus of the College of
 120 Forestry in the Ranichauri village. The RNC site is a Climate Monitoring station managed by the
 121 India Meteorological Department (IMD). It is a mountain background remote observatory
 122 (Sebastian et al., 2021b) and located about 70 km to the northeast of Rishikesh city, about 100 km
 123 to the northwest of the Srinagar city, and about 100 km to the east of Dehradun. Here, particle
 124 number size distributions in the size range from 10 nm to 757 nm (30 size bins) is measured using
 125 a differential mobility particle sizer (DMPS, Finnish Meteorological Institute assembled) from
 126 December 2016 to September 2018 are used (Sebastian et al., 2021b). The DMPS consisted of a
 127 Vienna-type differential mobility analyzer (DMA) that classifies the charged particles according
 128 to their electrical mobility and a TSI 3772 condensation particle counter (CPC) that counts
 129 particles of the selected mobility. The sample air was drawn inside through a stainless-steel inlet
 130 tube of about 2 meters in length and dried to less than 40% relative humidity with a Nafion dryer
 131 (Perma Pure model MD-700-48). Diffusion losses in the inlet and inside the DMPS instrument
 132 were considered in the data inversion. The inversion method was identical to that presented by
 133 Wiedensohler et al. (2012) for the Finnish Meteorological Institute (FMI) DMPS.

134 Mukteshwar observation site (MUK, 29.43° N, 79.62° E, 2180 m amsl) is located in the
135 Nainital district of Uttarakhand state in the southern slope of the Central Himalaya. The
136 Mukteshwar village is situated 3 km to the northeast of the measurement site at a similar altitude
137 with ~800 inhabitants (Census of India, 2011). MUK can be considered a mountain background
138 site, with the annual mean black carbon (BC) concentration of 0.9 $\mu\text{g m}^{-3}$. The town of Almora
139 (1650 m amsl, 34,000 inhabitants) is located at about 16 km to the north, Nainital (1960 m amsl,
140 41000 inhabitants) is located at about 25 km to the southwest, and the city of Haldwani (424 m
141 amsl, 150,000 inhabitants) is located at about 32 km to the southwest to MUK. Delhi, the major
142 metropolitan city (215 m amsl, 16.8 million inhabitants), is located approximately 250 km to the
143 southwest. Systematic measurements of aerosol properties have been conducted at MUK since
144 2005 in Indo-Finnish cooperation with the Finnish Meteorological Institute (Hooda et al., 2018
145 and references therein). Here, we used only two years (January 2012 to December 2013) of
146 measurements of particle number size distributions in the size range of 10 nm to 757 nm (30 size
147 bins). The air sampling procedure was similar to that of the RNC observation site. More details of
148 the site and aerosol sampling can be found in Hyvärinen et al. (2009).

149 Delhi observation site (DEL, 28.64° N, 77.17° E, 215 m amsl) is located at CSIR-National
150 Physical Laboratory (NPL). Delhi, India's national capital and largest metropolitan city in South
151 Asia, is located in the northwestern Indo Gangetic Plain (IGP) in northern India. Delhi city has a
152 population of 16.8 million, with a population density of 11,320 km^{-2} (Census of India, 2011). The
153 Great Indian Desert (Thar Desert) of Rajasthan state is located to the southwest, hot central plains
154 to the south, and hilly regions to the north and east of Delhi. Long-range transported air masses
155 often influence Delhi's air quality from the northwest (agricultural residue burning from Punjab
156 and Haryana in October-November) and southwest (dust storms from Thar and Arabian Peninsula
157 in April-June) (Kanawade et al., 2020b; Srivastava et al., 2014). Wide Range Aerosol
158 Spectrometer (WRAS, manufactured by GRIMM, Germany), installed on the second floor of the
159 NPL main building, was used to measure particle number size distributions. WRAS consists of a
160 Scanning Mobility Particle Sizer (SMPS) and an Environmental Dust Monitor (EDM). GRIMM-
161 SMPS system consists of a Vienna-type monodisperse differential mobility analyzer (M-DMA).
162 DMA classifies the particle according to their electrical mobility, which is then counted using a
163 CPC. EDM uses an Optical Particle Counter (OPC), which works on the light scattering
164 technology for particle counting gives the particle number size distribution in the size range from

165 250 nm to 32 μm (Grimm and Eatough, 2009). The WRAS system uses a stainless-steel inlet tube
166 with an integrated Nafion drier to dry the aerosol samples. A detailed description of the site and
167 aerosol sampling is given elsewhere (Jose et al., 2021). Thus, the WRAS system gives the particle
168 number size distribution in the size range from 5.5 nm to 32 μm (72 size bins). The detailed
169 description and principle of the instrument are discussed elsewhere (Grimm and Eatough, 2009).
170 In this study, we used particle number size distributions in the size range of 5.14 nm to 1000 nm
171 from November 2011 to January 2013.

172 Mahabaleshwar observation site (MBL, 17.92° N, 73.65° E; 1378 m amsl) is located in the
173 small town named Mahabaleshwar in the forested Western Ghats range in the Satara district of
174 Maharashtra State. In MBL, a High-Altitude Cloud Physics Laboratory (HACPL) was established
175 by the Indian Institute of Tropical Meteorology (IITM), Pune, in 2012, to study monsoon clouds
176 in this region. HACPL site details are found elsewhere (Anil Kumar et al., 2021). Mahabaleshwar
177 town is a tourist attraction consisting of dense vegetation, residential houses, hotels, and a rural
178 market. Pune city is located on the leeward side of the Western Ghats about 100 km to the north,
179 Mumbai city is located approximately 250 km on the northwest, and Satara city is located
180 approximately 50 km to the southeast of Mahabaleshwar. Measurements of particle number size
181 distributions were carried out using the GRIMM-WRAS system. The detailed description and
182 principle of the instrument are discussed elsewhere (Grimm and Eatough, 2009). The WRAS has
183 a stainless-steel inlet tube with an integrated Nafion dryer to reduce the relative humidity to ~40%.
184 In this study, we used particle number size distributions in the size range of 5.14 nm to 1000 nm
185 from March 2015 to March 2016.

186 Hyderabad observation site (HYD, 17.46° N, 78.32° E; 542 m amsl), University of
187 Hyderabad, is located in the outskirts of Hyderabad urban city. HYD observation site details can
188 be found in Sebastian et al. (2021a). Briefly, particle number size distributions in size range from
189 10.9 to 514 nm (108 size bins) were measured using TSI SMPS, which consists of an electrostatic
190 classifier with a long differential mobility analyzer (TSI LDMA, model 3082) and a butanol CPC
191 (TSI, model 3772), on the second floor of the Earth Sciences building located in the University of
192 Hyderabad campus from April 2019 to March 2020. The scanning cycle of SMPS was 300
193 seconds, yielding a particle number size distribution every 5 minutes.

194 Thiruvananthapuram (Trivandrum) observation site (TVM, 8.55° N, 76.97°E, 3 m amsl) is
195 a tropical semi-urban coastal city with a population of ~1 million (Census of India, 2011), located

196 on the southwestern coast of the Indian peninsular. The observations were carried out at the Space
197 Physics Laboratory (SPL) within the Thumba Equatorial Rocket Launching Station, which is about
198 500 m due east of the Arabian Sea coast and 10 km northwest of the urban area of
199 Thiruvananthapuram. The experimental site is free from major industrial or urban activities (Babu
200 et al., 2016). TVM station is a part of the Aerosol Radiative Forcing over India (ARFI) project
201 network of the Indian Space Research Organisation - Geosphere-Biosphere Program (ISRO-GBP).
202 Measurements of particle number size distributions in size range from 14.6 nm to 661.2 nm (108
203 size bins) were made using TSI SMPS, which consists of an electrostatic classifier with an LDMA
204 (3081) and a water-based CPC (3786) from January 2013 to January 2014. The ambient air was
205 sampled from a height of 3 m above ground level through a manifold inlet fitted with a PM_{10} size
206 cut impactor at 16.67 LPM flow rate. Subsequently, the flow was distributed among various
207 aerosol instruments connected with electrically conductive tubing. A diffusion dryer (Make: TSI,
208 Model: 3062) employing silica gel was used to restrict high relative humidity conditions. More
209 details about the site and prevailing meteorology are described in Babu et al. (2016).

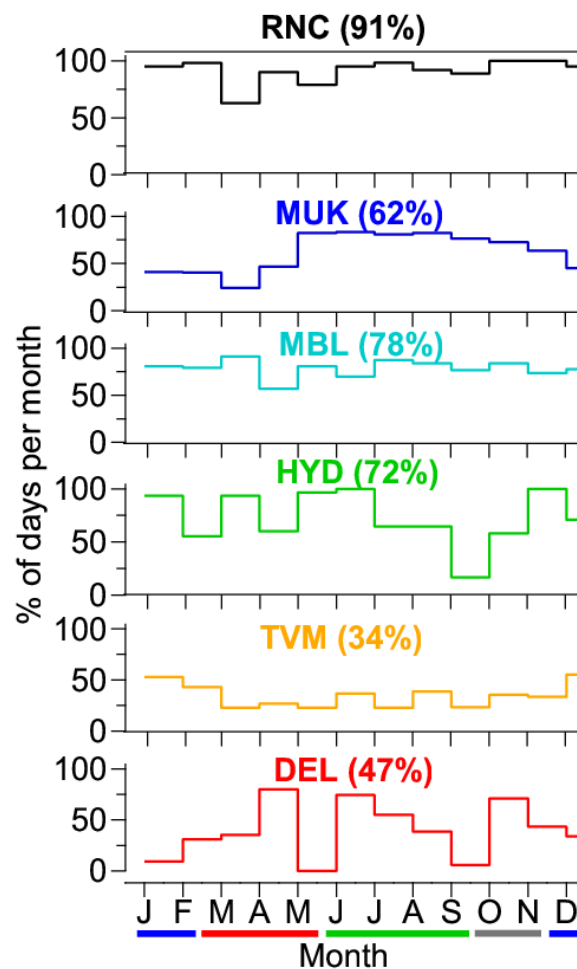
210 Particle number size distributions are categorized by season. We have defined four seasons
211 as indicated in Table 2. The overall particle number size distribution data coverage was adequate
212 (>60 %) at the RNC, MUK, MBL, and HYD sites (Fig. 2) for determining the main seasonal and
213 annual features of particle number size distributions and NPF characteristics. The data coverage at
214 TVM (34%) and DEL (47%) was lower. We also analyzed the number concentration of three sub-
215 micron aerosol modes: Aitken mode (25-100 nm), accumulation mode (100-514 nm), and total
216 particles (<514 nm). Figure S1 shows the three-day air mass backward trajectories arriving at 500
217 m above the ground level at all sites for winter, pre-monsoon, monsoon and post-monsoon seasons.
218 RNC and MUK generally experience a mixture of relatively cleaner free tropospheric air and
219 polluted air from the highly polluted Indo-Gangetic Plain. MBL experiences marine air masses
220 during pre-monsoon and monsoon seasons while continental air masses during post-monsoon and
221 winter. HYD experiences mixed marine and continental air masses from the northeast during post-
222 monsoon and winter seasons while from southeast and west during pre-monsoon and monsoon,
223 respectively. TVM predominantly experiences air masses of marine origin throughout the year,
224 with continental influence during the winter season. DEL mostly experiences air masses from the
225 northwest during pre-monsoon, post-monsoon and winter seasons and from southeast and
226 southwest during monsoon season.

227

228 **Table 2.** Seasons are defined in the analysis and average weather conditions.

Season	Months	Comments
Winter	December, January, February	Cold and dry
Pre-monsoon	March, April, May	Hot and dry
Monsoon	June, July, August, September	Warm, humid, and wet
Post-monsoon	October, November	Cool and humid

229



230

231 **Figure 2.** Particle number size distributions data coverage (% of days/month) at the sites. The
232 values in the bracket indicate total data coverage. The blue, red, green, and grey colored thick lines
233 indicate winter, pre-monsoon, monsoon, and post-monsoon months. Note that measurements are
234 from different time periods for each site (refer to Table 1).

235

236 2.2 New particle formation event classification and features

237 We classified observation days into three types of events: NPF event day, non-event day,
238 and undefined event day using visual inspection of the particle number size distributions following
239 the methodology given by Dal Maso et al. (2005). A day was classified as an NPF event day by
240 the presence of a distinctly new mode of particles with a diameter smaller than 25 nm and steady
241 growth in diameter of this new mode such that the particle number size distributions display a
242 noontime "banana" shaped aerosol growth. The particle mode diameter (i.e., the local maximum
243 of the particle number size distribution) was obtained by fitting a log-normal distribution to the
244 measured particle number size distribution. A day without any evidence of a distinctly new mode
245 of particles diameter smaller than 25 nm was identified as a non-event day. Those days, which
246 were difficult to be classified as any one of the above two event types, were identified as undefined
247 event days. For NPF events, the particle growth rate was calculated by fitting a first-order
248 polynomial line through growing particle mode diameter between the smallest detectable size
249 (SDS) of the instrument (e.g., 10 nm for RNC) and 25 nm as a function of time and calculating its
250 slope ($GR_{SDS-25nm}$). The formation rate of a particle at the SDS (J_{SDS}) was also found using the
251 simplified approximation of the General Dynamic Equation (GDE), describing the evolution of
252 the particle number size distribution as given below;

253

$$254 \quad J_{SDS} = \frac{dN_{SDS-25}}{dt} + F_{CoagS} + F_{growth} \quad (1)$$

255

256 where the first term in Eq. (1) is the rate of the change of nucleation mode particle number
257 concentrations, the second term is the coagulation loss of nucleation mode particles, and the third
258 term is the flux out of the size range of SDS-25 nm, i.e., condensational growth (Dal Maso et al.,
259 2005). A direct comparison of J_{SDS} and $GR_{SDS-25nm}$ between the sites is not possible because of
260 the different size ranges covered by the instruments.

261

262 2.3 Increase in CCN concentrations from NPF

263 The increase in CCN concentrations from any given NPF event can be estimated by
264 comparing the CCN concentration before the event ($N_{CCNprior}$) and the maximum CCN
265 concentration during the event (N_{CCNmax}) following the methodology developed by Kerminen et
266 al. (2012), which we modified further. In typical ambient in-cloud supersaturations, the total

267 number of particles from 50 nm to >100 nm can be considered as a proxy for CCN concentrations
 268 assuming fixed chemical composition (Westervelt et al., 2013; Kerminen et al., 2012). $N_{CCN_{prior}}$
 269 was chosen to be a one-hour average concentration of particles larger than 50 nm (and 100 nm)
 270 just before the start of the NPF event. The start of the NPF event is the time when nucleation mode
 271 particle number concentrations increase rapidly during an NPF event. $N_{CCN_{max}}$ was taken as a
 272 maximum one-hour average concentration of particles larger than 50 nm (and 100 nm) during the
 273 event. The $N_{CCN_{max}}$ is not the best representation of CCN concentration after the NPF event
 274 because it is not possible to estimate the end of an NPF event. But it gives a rough estimate of the
 275 observed maximum number of primary and secondary particles present in the atmosphere during
 276 an event (Kerminen et al., 2012). For non-event days, the seasonally averaged start of the NPF
 277 event time was chosen to calculate $N_{CCN_{prior}}$. $N_{CCN_{max}}$ on non-event days was taken similar to NPF
 278 event days, as a maximum one-hour average concentration of particles larger than 50 nm (and 100
 279 nm). The second term in Eq. (2) gives approximate CCN concentrations from processes other than
 280 NPF. Then, the absolute increase in CCN concentration from NPF is calculated as given below,

$$281$$

$$282 \text{CCN increase} = (N_{CCN_{max}} - N_{CCN_{prior}})_{NPF\text{event}} - (N_{CCN_{max}} - N_{CCN_{prior}})_{\text{non-events}} \quad (2)$$

$$283$$

284 The first term on the right-hand side in Eq. (2) indicates the CCN increase during an NPF event,
 285 while the second term indicates the CCN increase during a non-event. But the atmospheric
 286 condition on non-event days is generally different from NPF event days; therefore, the calculated
 287 increase in CCN concentrations from NPF may be imprecise.

288

289 **3. Results and discussion**

290 **3.1 Variability in particle number size distributions and number concentrations**

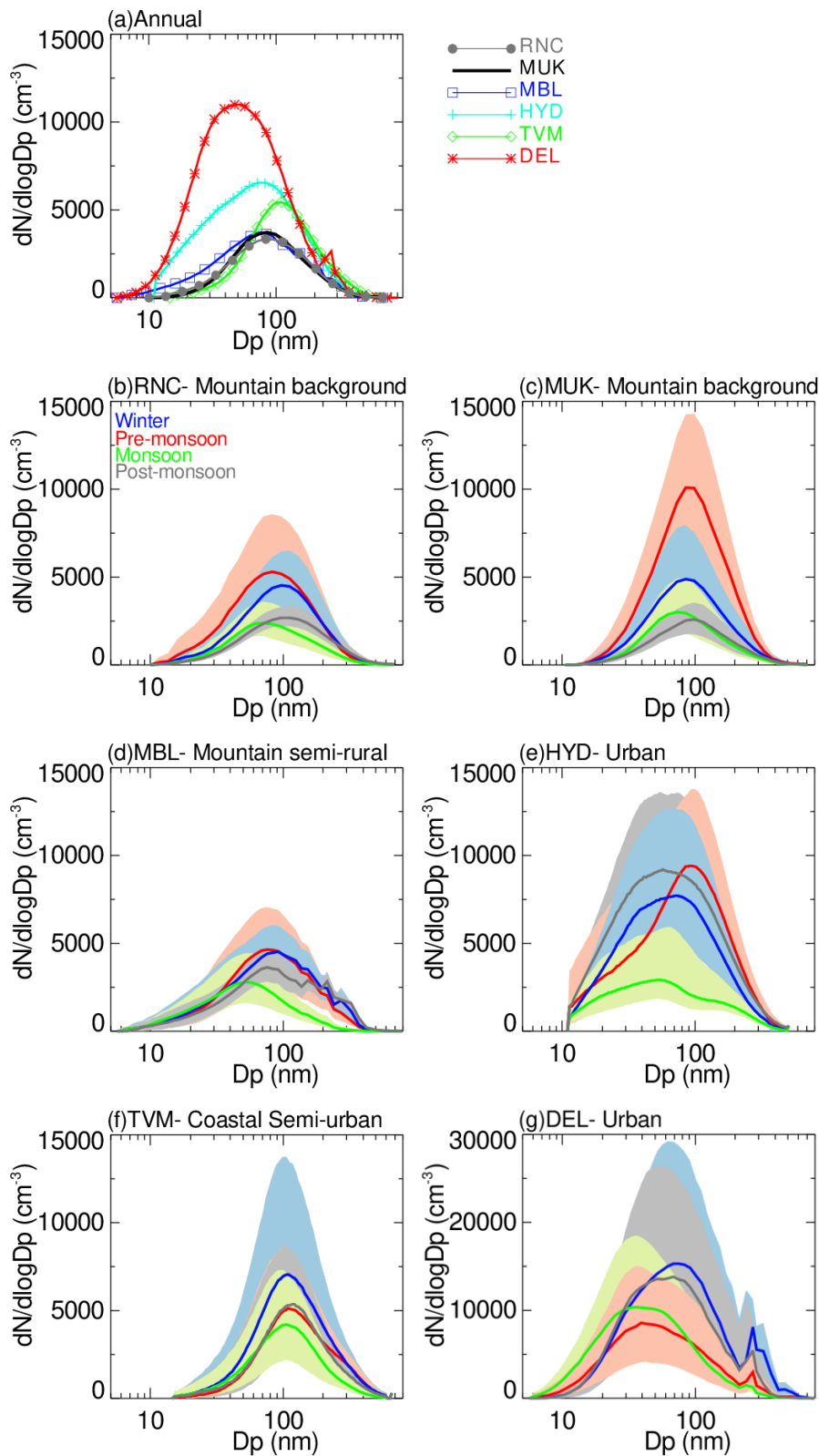
291 Figure 3 shows the annual and seasonal median and 25th and 75th percentile values of
 292 particle number size distributions at all the sites. The thick line represents the median value,
 293 whereas the shaded area indicates particle number size distribution between 25th and 75th
 294 percentiles. The mountain sites (RNC, MUK, and MBL) all show similar mode diameters, with
 295 the lowest concentrations at RNC. Amongst urban areas (HYD, TVM, and DEL), TVM has the
 296 largest mode diameter, which is frequently influenced by the influx of marine air masses
 297 containing high moisture and coarser sea salt aerosols (Babu et al., 2016) (Fig. 3a). The peak

298 number concentration of PNSDs is the highest in pre-monsoon (MAM) than in other seasons at
299 the mountain background sites RNC and MUK (Fig. 3b-c), while it was similar in winter and pre-
300 monsoon at MBL (Fig. 3d). These elevated concentrations are accompanied by a smaller mode
301 diameter of the Aitken mode particles. The highest number concentration is attributed to the
302 frequent occurrence of NPF in these locations in pre-monsoon (Sebastian et al., 2021b; Neitola et
303 al., 2011). The contribution of newly formed particles to total particles is also visible in the 75th
304 percentile PNSDs at these sites. The number size distributions of particles were significantly the
305 lowest in monsoon and post-monsoon.

306 The median number size distribution of particles at HYD is the highest in pre-monsoon
307 and post-monsoon (Fig. 3e). The highest particle number concentrations in pre-monsoon and post-
308 monsoon can be attributed to the frequent occurrence of NPF in these seasons at the site. The
309 influence of NPF is also noticeable in the 75th percentile PNSDs. The PNSD is consistently the
310 lowest in monsoon, attributed to the wet scavenging of particles. The concentrations of Aitken and
311 accumulation mode particles are the highest in winter compared to the other seasons. The mode
312 diameter of PNSDs at TVM is comparatively similar in all seasons (Fig. 3f). At DEL, the mode
313 diameter of PNSDs is the highest in winter compared to the other seasons (Fig. 3g). The shallow
314 boundary layer height, stagnant atmospheric conditions, and high emission rates of aerosol
315 precursors in winter (Kanawade et al., 2020b) allow particles to stay close to the surface and grow
316 larger under high relative humidity and high condensable vapor concentrations. The median PNSD
317 is consistently the lowest in monsoon at TVM due to extensive wet scavenging. The strong
318 seasonality in PNSDs is similar to those reported earlier in India (Hooda et al., 2018; Komppula
319 et al., 2009; Gani et al., 2020; Kanawade et al., 2014a). The uni- and bi-modal parameters of the
320 particle number size distributions presented in Fig. 3 are tabulated in Table S1.

321

322



323

324

325

326

327 **Figure 3.** (a) Annual and (b-g) seasonal median particle number size distributions at all the sites.

328 The solid line indicates the median, and the light-colored shading indicates 25th and 75th percentile

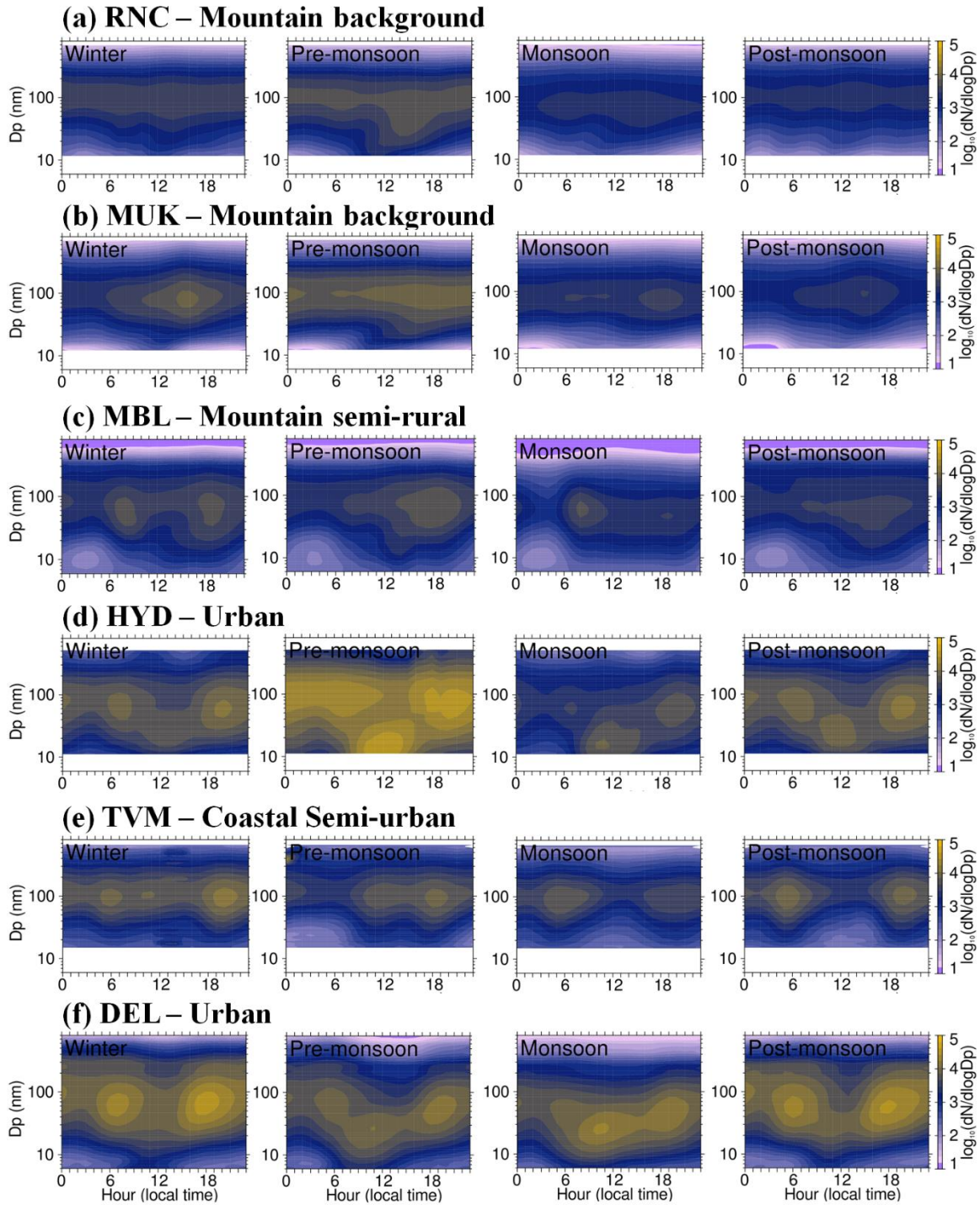
329 distributions. The blue line and shading indicate winter (DJF), red line and shading indicate pre-
330 monsoon (MAM), green line and shading indicate monsoon (JJAS), and grey line and shading
331 indicate post-monsoon season (ON). Note that the y-axis scale is different for the DEL site. Note
332 that measurements are from different time periods for each site (refer to Table 1).

333

334 Figure 4 shows the average observed PNSDs evolving over the day for each season, as a
335 contour plot, at all the sites. For the mountain background sites RNC and MUK, the average
336 seasonal contour plot indicates daytime NPF in pre-monsoon. However, winter, monsoon, and
337 post-monsoon had the lowest concentrations of smaller particles that are not associated with NPF.
338 For MBL, NPF occurred in winter, pre-monsoon, and post-monsoon. For all urban sites (HYD,
339 TVM, and DEL), the average seasonal contour plot indicates the highest concentration of particles
340 in morning and evening peak traffic hours, in addition to daytime NPF. In Section 3.2, we have
341 considered this high particle concentration from evening peak traffic while investigating the
342 frequency of occurrence of NPF and its contribution to CCN concentrations.

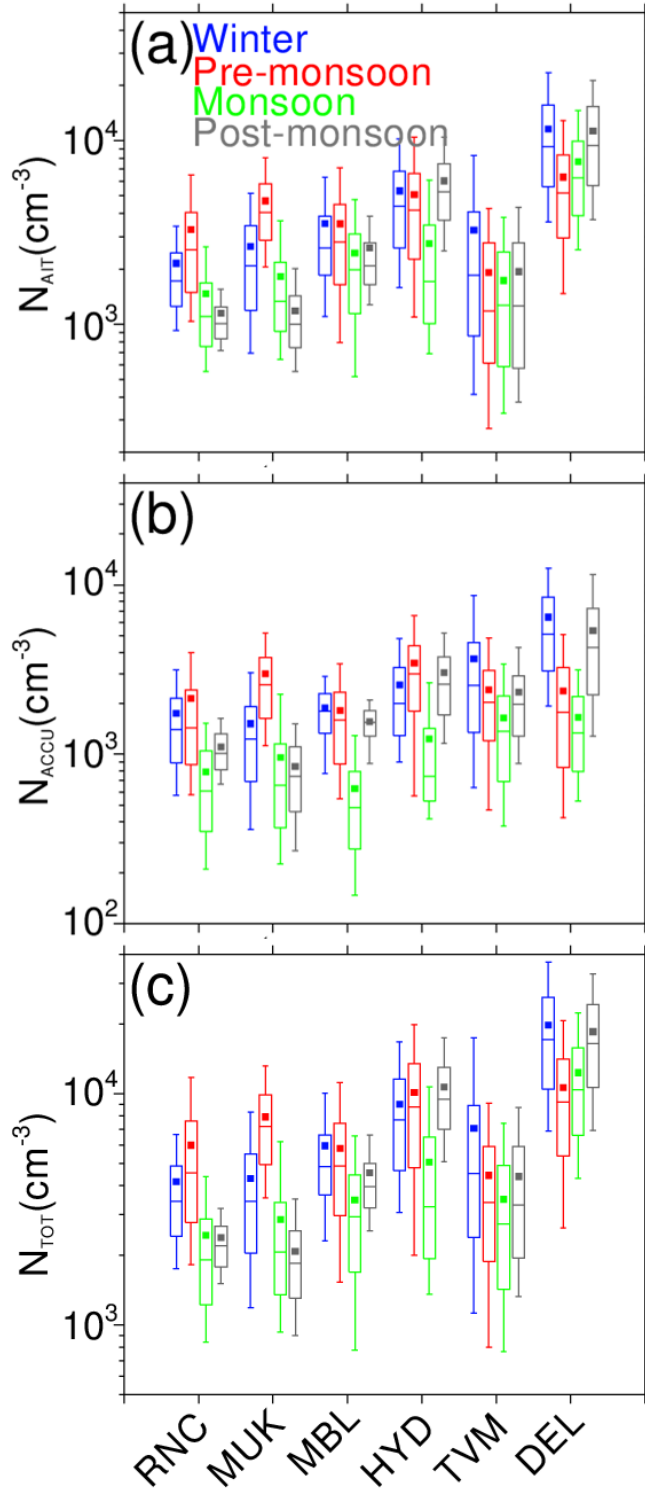
343

344



345
 346 **Figure 4.** The diurnal-seasonal median particle number size distributions at all the sites; a)
 347 Ranichauri, b) Mukteshwar, c) Mahabaleshwar, d) Hyderabad, e) Thiruvananthapuram, and f)
 348 Delhi. Note that measurements are from different time periods for each site (refer to Table 1).
 349

350 Figure 5 shows the box-whisker plot of the seasonal number concentrations of Aitken,
351 accumulation, and total particles at all the sites. The periods of study are different for all the sites,
352 where direct comparison of particle number concentrations is not possible. The median Aitken
353 mode particle number concentrations are the lowest at RNC ($1.4 \times 10^3 \text{ cm}^{-3}$) and the highest at DEL
354 ($7.1 \times 10^3 \text{ cm}^{-3}$). The median accumulation mode particle number concentrations are the lowest at
355 MUK ($0.9 \times 10^3 \text{ cm}^{-3}$) and the highest at DEL ($2.4 \times 10^3 \text{ cm}^{-3}$). The total particle number
356 concentrations are the lowest at MUK ($2.7 \times 10^3 \text{ cm}^{-3}$) and the highest at DEL ($12.5 \times 10^3 \text{ cm}^{-3}$).
357 The median particle number concentrations are about 5-fold higher in urban locations (HYD,
358 TVM, and DEL) than mountain sites (RNC, MUK, and MBL). Overall, the size-segregated particle
359 number concentrations show strong seasonal spatial variability, with the lowest concentrations at
360 the mountain sites and the highest at the urban sites. Further, the size-segregated particle number
361 concentrations also show the large variability in each urban location than the mountain sites. Next,
362 we discuss the seasonality in the number concentration of Aitken, accumulation, and total particles
363 in all locations to understand space- and time-varying heterogeneity in particle number
364 concentrations.

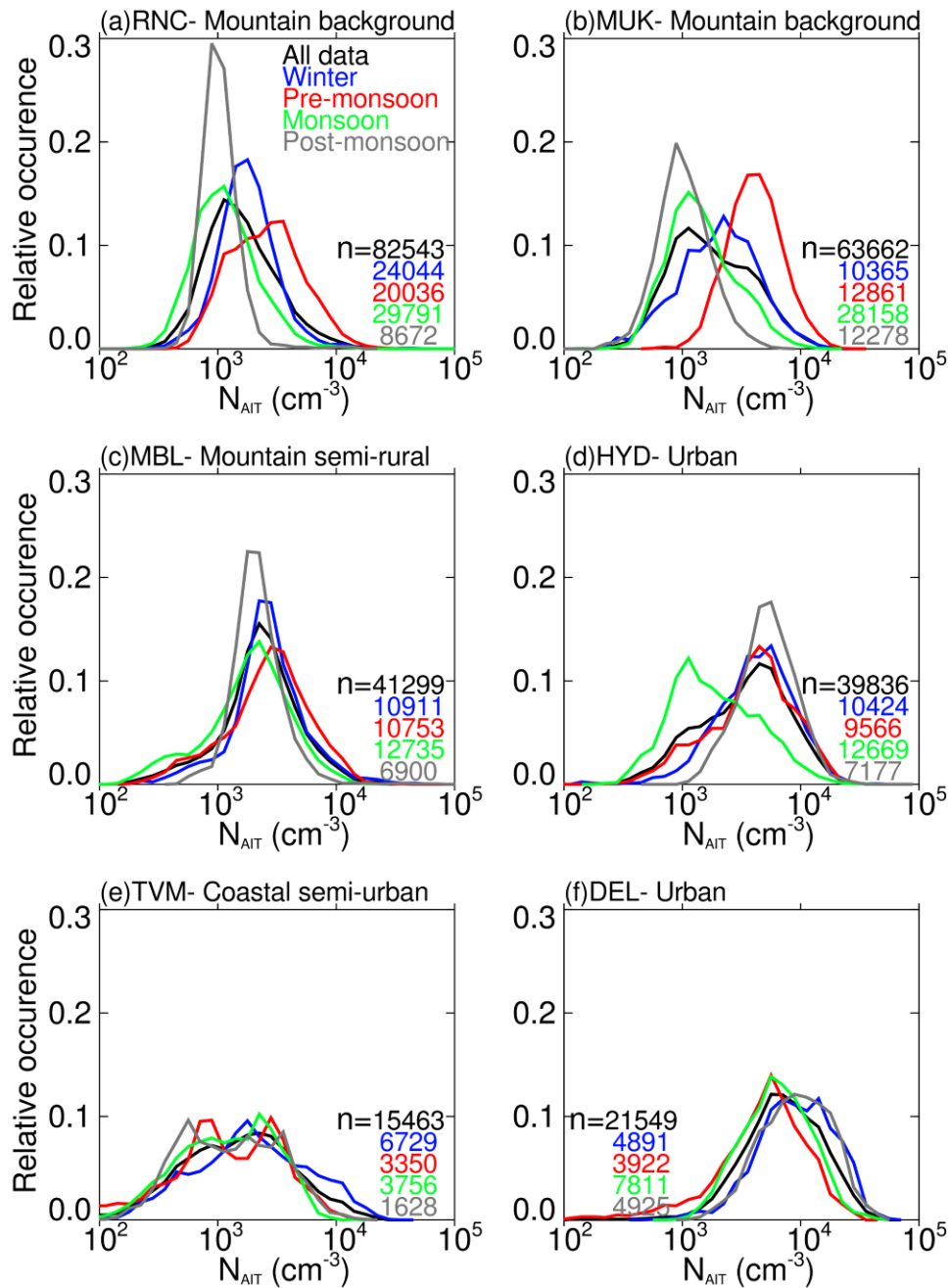


365
 366 **Figure 5.** Box-whisker plot of seasonal number concentrations of (a) Aitken mode (b)
 367 accumulation mode, and (c) total particles using the entire data. The blue, red, green, and grey
 368 color indicate winter (DJF), pre-monsoon (MAM), monsoon (JJAS), and post-monsoon (ON)
 369 months. The filled square indicates the mean, horizontal line indicates the median, the top and

370 bottom of the box indicate 25th and 75th percentile values, and the top and bottom whiskers indicate
371 10th and 90th percentile values. Note that measurements are from different time periods for each
372 site (refer to Table 1).

373
374 The relative occurrence of the number concentrations of size-segregated (Aitken and
375 accumulation) particles was calculated to determine the maximum concentrations of a given
376 particle mode in different seasons at all sites. The histograms of the relative occurrence of Aitken
377 mode particle number concentrations at all the sites are presented in Figure 6(a-f). The mountain
378 background sites RNC and MUK show a similar seasonality in number concentration histograms
379 of Aitken mode particles, with the highest concentrations in the pre-monsoon season. The lowest
380 concentrations are observed in monsoon and post-monsoon due to increased removal of particles
381 by wet-scavenging. MBL does not show notable seasonality in the number concentration
382 histograms of Aitken mode particles. HYD, TVM, and DEL are urban environments but show
383 different seasonality in the number concentration histograms of Aitken mode particles. DEL shows
384 the highest Aitken mode particle number concentrations in winter, and post-monsoon, TVM show
385 the highest concentrations in winter. In contrast, HYD shows comparable number concentrations
386 in winter, pre-monsoon, and post-monsoon. The highest Aitken mode number concentrations in
387 pre-monsoon at mountain-background sites are attributed to the high frequency of NPF occurrence
388 in pre-monsoon (see Sect. 3.2.1). The highest Aitken mode number concentrations in winter at
389 urban sites can be explained by the high pre-existing particle concentration. DEL has the highest
390 concentration of Aitken mode particles during winter owing to the anthropogenic sources and the
391 stagnant atmospheric conditions during the season (Kanawade et al., 2020b). The difference in
392 seasonality in the number concentration histograms of Aitken mode particles can be explained by
393 the differences in the atmospheric conditions (e.g., prevailing synoptic air masses, mesoscale
394 processes such as atmospheric boundary layer dynamics, and particle removal processes) and
395 considerable heterogeneity in aerosol composition (natural versus anthropogenic aerosol emission
396 sources); DEL is representative of a sub-tropical climate, HYD is representative of a tropical
397 climate, and TVM is representative of a tropical-coastal climate.

398
399

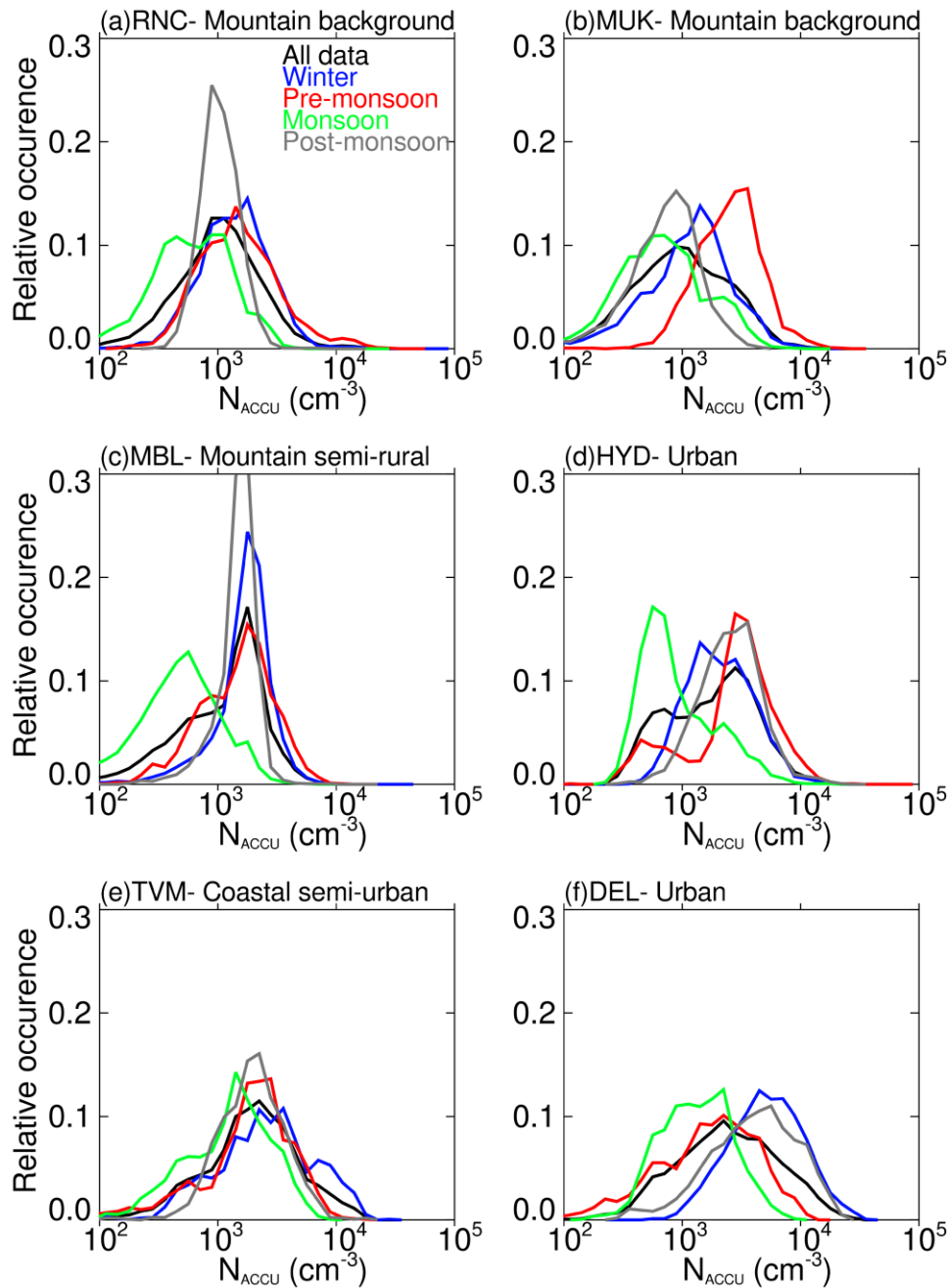


400

401 **Figure 6.** Histogram of the relative occurrence of Aitken mode particle number concentrations at
 402 the sites. The concentration bins are logarithmically spaced in the x-axis, and the y-axis shows the
 403 relative occurrence of values in each bin compared to the total number of valid observations. The
 404 black, blue, red, green, and grey lines indicate all data, winter (DJF), pre-monsoon (MAM),
 405 monsoon (JJAS), and post-monsoon (ON), respectively. n indicates the number of 10 minutes
 406 averaged valid data points. Note that measurements are from different time periods for each site
 407 (refer to Table 1).

408
409
410
411
412
413
414
415
416
417
418
419
420
421
422
423
424
425
426
427
428
429

Similar histograms of accumulation mode particles are presented in Fig. 7(a-f). The seasonality in accumulation mode particles is slightly different as compared to Aitken mode particles at some sites. RNC shows similar number concentration histograms of accumulation mode particles in winter and pre-monsoon instead of dissimilar histograms for Aitken mode particles. The number concentration histograms of accumulation mode particles at MUK are similar to Aitken mode particles. MBL shows similar number concentration histograms in winter, pre-monsoon, and post-monsoon, with the lowest concentrations in monsoon due to wet scavenging. Among the urban sites, DEL shows the highest accumulation mode concentrations in post-monsoon and winter. TVM and HYD show the highest accumulation mode concentrations in winter and post-monsoon, respectively. The seasonality in total particles was also similar to Aitken mode particles, indicating that Aitken mode particles constituted the most considerable fraction of total particles at all the sites (Figure S2). However, it is difficult to separate a fraction of Aitken or accumulation mode particles that originated from NPF from that of the primary emissions, especially in urban areas where the primary emission rates of aerosols are very high (Thomas et al., 2019). The survival probability of newly formed particles to >50-100 nm size depends on many factors such as the frequency and intensity of the NPF occurrence, availability of condensable vapors, pre-existing particles, and atmospheric conditions. In Sect. 3.2.3, we estimate the absolute increase of CCN concentrations from NPF following the methodology given by Kerminen et al. (2012) and modified to calculate CCN concentrations for any given NPF event.



430

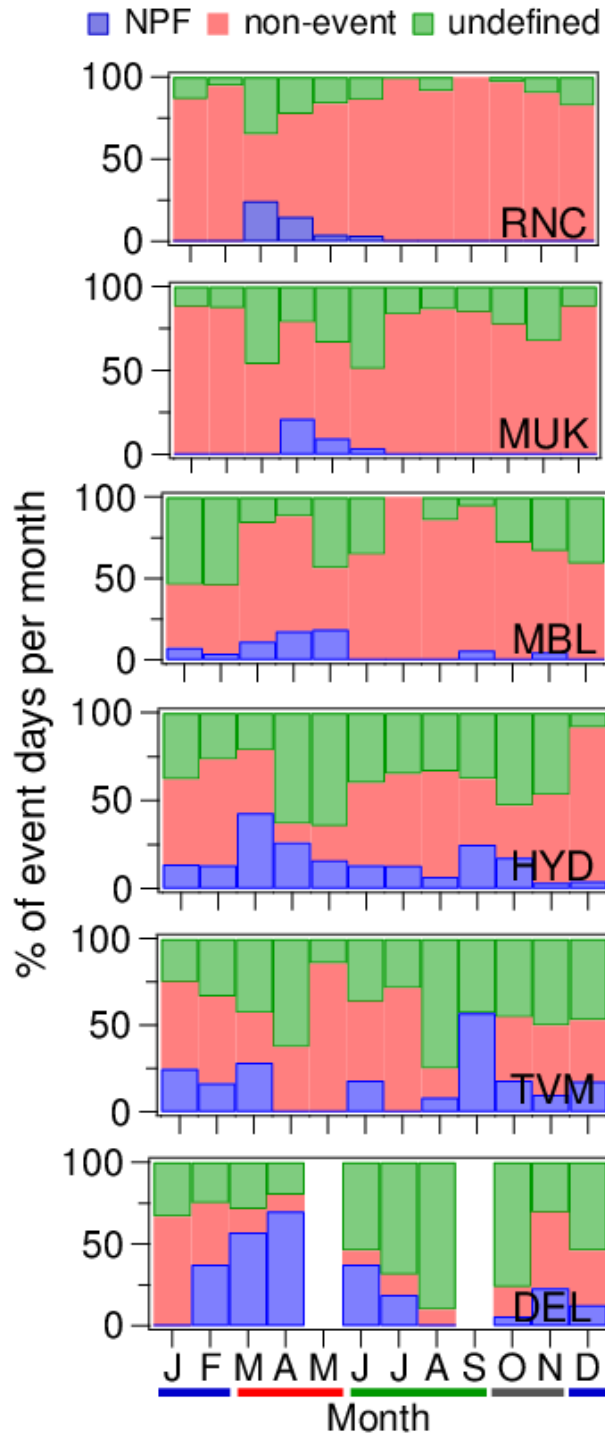
431 **Figure 7.** Histogram of the relative occurrence of accumulation mode particle number
 432 concentrations at the sites. The concentration bins are logarithmically spaced in the x-axis, and the
 433 y-axis shows the relative occurrence of values in each bin compared to the total number of valid
 434 observations. The black, blue, red, green, and grey lines indicate all data, winter (DJF), pre-
 435 monsoon (MAM), monsoon (JJAS), and post-monsoon (ON), respectively. n indicates the number
 436 of 10 minutes averaged valid data points. Note that measurements are from different time periods
 437 for each site (refer to Table 1).

438
439
440
441
442
443
444
445
446
447
448
449
450
451
452
453
454
455
456
457
458
459
460
461
462

3.2 New particle formation and its contribution to CCN concentrations

3.2.1 NPF event characteristics

The frequency of occurrence of NPF events, the particle formation rate of nucleation mode particles (J_{SDS}), and the particle growth rate of nucleation mode particles ($GR_{\text{SDS-25nm}}$) are typically derived to quantify the NPF (Kerminen et al., 2018; Nieminen et al., 2018; Kulmala et al., 2004). These NPF characteristics are closely associated with aerosol precursor concentrations, pre-existing aerosol particles, and atmospheric conditions. As a result, the frequency of occurrence of NPF events varies from one location to another as well as seasonally. NPF is thought to occur frequently during the spring (pre-monsoon) and rarely during the winter (Kanawade et al., 2012; Dal Maso et al., 2005; Nieminen et al., 2018). However, NPF events were also observed frequently during the thermal winter (Kulmala et al., 2004; Pikridas et al., 2012) and fall (September, October, and November) (Rodríguez et al., 2005). These studies indicate that there is no universal pattern in the occurrence of NPF events. Figure 8 shows the percentage of NPF, non-event, and undefined event days based on valid observation days at all the sites. Out of a total of 586 valid observation days at RNC, NPF events occurred on 21 days (3.9%), whereas 493 (83.7%) days were non-event days. Out of a total of 440 valid observation days at MUK, NPF events occurred on 13 days (2.9%), whereas 321 (73.1%) days were non-event days. Out of a total of 281 valid observation days at MBL, NPF events occurred on 16 days (5.9%), whereas 188 (66.1%) days were non-event days. Out of a total of 270 valid observation days at HYD, NPF events occurred on 38 days (16.3%), whereas 124 (44.8%) days were non-event days. Out of a total of 133 valid observation days at TVM, NPF events occurred on 23 days (16.6%), whereas 55 (41.4%) days were non-event days. Out of a total of 139 valid observation days at DEL, NPF events occurred on 39 days (28.1%), whereas 30 (21.1%) days were non-event days. The frequencies of NPF occurrence at all six sites are tabulated in Table S2.



463
 464 **Figure 8.** Monthly percentage of occurrence of NPF, non-event, and undefined events days based
 465 on total valid observations days at all the sites. The blue, red, green, and grey colored thick lines
 466 indicate winter, pre-monsoon, monsoon, and post-monsoon months. Note that measurements are
 467 from different time periods for each site (refer to Table 1).

468
469
470
471
472
473
474
475
476
477
478
479
480
481
482
483
484
485
486
487
488
489
490
491
492
493
494
495
496
497
498

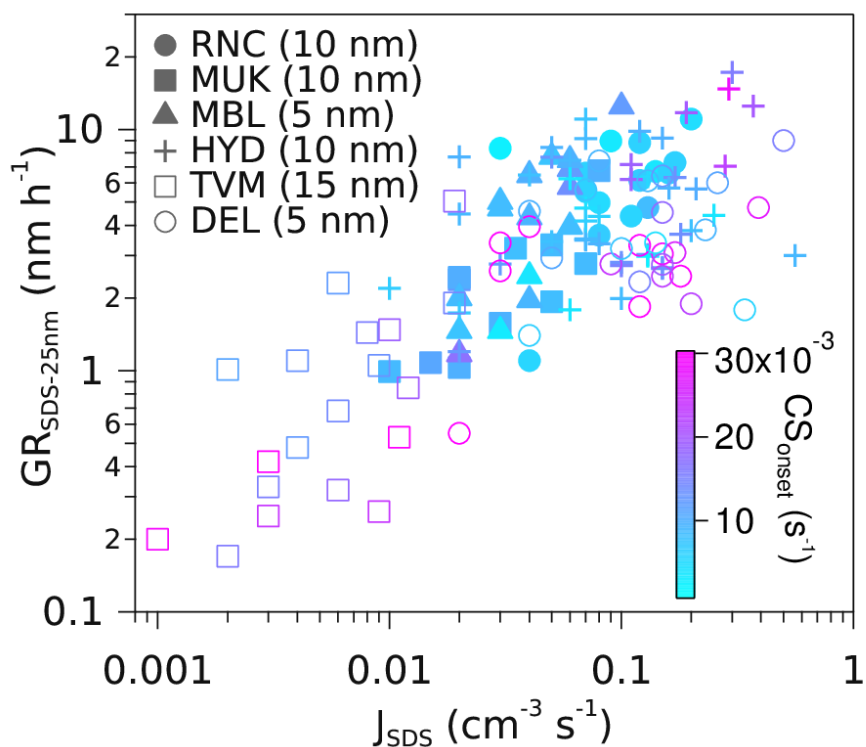
3.2.2 Particle formation rate and growth rate

Overall, the frequency of occurrence of NPF is the highest in pre-monsoon as compared to other seasons. There is also an exception to this, with the highest frequency of NPF occurrence in the late monsoon (September) at TVM. Babu et al. (2016) have reported that NPF events over this site occurred due to a mixing of contrasting air masses due to the combined effect of mesoscale land-sea breeze circulation and local ABL dynamics. Though prevailing air masses are oceanic, the wind speeds and total rainfall were lower during September than other monsoonal months. A cleaner synoptic air mass (i.e., lower background concentrations and condensation sink), combined with the occurrence of well-defined mesoscale land-sea breeze transitions and horizontal convergence of contrasting air masses during September, was responsible for the highest NPF frequency. Amongst the sites, the mountain-background sites in the Western Himalaya (RNC and MUK) have the lowest annual mean frequency of occurrence of NPF (3.9% and 2.9%, respectively), with the highest seasonal frequency of occurrence of NPF in pre-monsoon. Previous studies also showed the infrequent occurrence of NPF at RNC (Sebastian et al., 2021b) and MUK (Neitola et al., 2011), with the highest frequency in pre-monsoon. The highest NPF frequency in pre-monsoon was connected to the planetary boundary layer uplifting to the measurement site elevation that appeared to transport aerosol precursors from nearby polluted lower-altitude regions (Hooda et al., 2018; Raatikainen et al., 2014). However, NPF occurred frequently (39%) at the Nepal Climate Observatory-Pyramid (NCO-P) site in the Eastern Himalaya (Venzac et al., 2008). A recent study also observed a very high NPF frequency (69%) at NCO-P from November to December when cleaner conditions prevailed, with little transportation from the polluted lower-altitude regions (Bianchi et al., 2021). They showed that up-valley winds bring gaseous aerosol precursors to higher altitudes. These precursors are oxidized into compounds of very low volatility and are subsequently converted into new particles during their transport to the site. The above discussion indicates that RNC and MUK mountain-background sites in the Western Himalayas are strikingly different from the NCO-P site in the Eastern Himalayas (Bianchi et al., 2021). The annual NPF frequency at RNC and MUK is lower than MBL and the high-altitude sites in Europe (Nieminen et al., 2018). DEL has the highest frequency of occurrence of NPF events in pre-monsoon (63.8%), followed by HYD (28.4%) and MBL (15.9%). TVM coastal semi-urban site witnesses frequent NPF events under the influence of continental air masses. As the air masses

499 change from continental to the mixed or marine origin, the NPF event frequency decreases (Babu
500 et al., 2016). NPF was also observed commonly at other urban sites in India (Kanpur and Pune)
501 under a high source of aerosol precursors when pre-existing particle concentrations reduced
502 sufficiently due to dilution (Kanawade et al., 2020a; Kanawade et al., 2014b). While the severe air
503 pollution episode in Delhi in November 2016 suppressed the NPF, the co-condensation of vapors
504 of anthropogenic origin along with water onto primary particles assisted the rapid particle growth
505 (1.6 to 30.3 nm h^{-1}) (Kanawade et al., 2020b). The emission of precursor compounds from traffic
506 and other sources in Beijing, China, also contributed significantly to the molecular cluster
507 formation, particle growth and secondary aerosol mass formation, leading to haze formation under
508 favorable meteorological conditions (Kulmala et al., 2021). In Europe, the atmospheric conditions
509 (such as the solar radiation and relative humidity) appear to dictate the NPF occurrence at rural
510 sites, whereas the increased concentrations of precursor gases are more important for the
511 occurrence of NPF in urban areas (Bousiotis et al., 2021). This explains why NPF occurs more
512 frequently in urban areas than rural, remote or high-altitude locations (Guo et al., 2020; Nieminen
513 et al., 2018; Sellegri et al., 2019). This also indicates that the balance between the precursor
514 concentration and pre-existing particles plays a vital role in the NPF occurrence. Owing to large
515 spatial heterogeneity in aerosol precursor emissions and background aerosol concentrations in
516 India, the chemical species contributing to aerosol nucleation and growth is unidentified
517 (Kanawade et al., 2021).

518 Figure 9 shows the scatter plot of the J_{SDS} and the $\text{GR}_{\text{SDS-25nm}}$ as a function of condensation
519 sink at each site. A fairly good correlation between J_{SDS} and $\text{GR}_{\text{SDS-25nm}}$ at each site (Pearson
520 correlation coefficient of 0.48, 0.78, 0.85, 0.33, 0.68, and 0.18 at RNC, MUK, MBL, HYD, TVM,
521 and DEL, respectively) indicates that J_{SDS} and $\text{GR}_{\text{SDS-25nm}}$ are strongly coupled. The large scatter
522 in data points is a result of important factors influencing the NPF, such as nucleation mechanisms
523 (Dunne et al., 2016), the availability of other condensable vapors that are needed to stabilize
524 molecular clusters containing sulfuric acid (Kirkby et al., 2011; Schobesberger et al., 2015), and
525 atmospheric conditions (Bousiotis et al., 2021). A recent study showed that amines stabilize the
526 nucleating cluster while organics contribute to higher concentrations of condensable vapors,
527 particularly in urban areas (Xiao et al., 2021). The mean particle formation rates and growth rates
528 for all six sites are tabulated in Table S2. Considering all the sites, $\text{GR}_{\text{SDS-25nm}}$ during NPF events
529 varied from 0.2 to 17.2 nm h^{-1} . Overall, J_{SDS} and $\text{GR}_{\text{SDS-25nm}}$ are within the observed large range of

530 values in diverse environments in India and elsewhere (Nieminen et al., 2018; Kerminen et al.,
 531 2018; Kulmala et al., 2004). Expectedly, the mean condensation sink at the start of the NPF event
 532 is higher at urban sites than the mountain sites. The mean condensation sink at urban sites
 533 ($16.1 \times 10^{-3} \text{ s}^{-1}$) was twice as compared to mountain sites ($7.9 \times 10^{-3} \text{ s}^{-1}$). A previous study also
 534 showed that the higher pre-existing particles at Kanpur than at Pune suppressed the particle
 535 formation rate but favored the particle growth under high concentrations of condensable vapors
 536 (Kanawade et al., 2014b)



537
 538 **Figure 9.** Scatter plot of the particle formation rate and the growth rate as a function of
 539 condensation sink at each site. The condensation sink at the start of the event (CS_{onset}) is taken as
 540 a one-hour average CS just before the start of the NPF event. The lowest nucleation mode
 541 detectable size at each site is shown in the bracket. Note that measurements are from different time
 542 periods for each site (refer to Table 1).

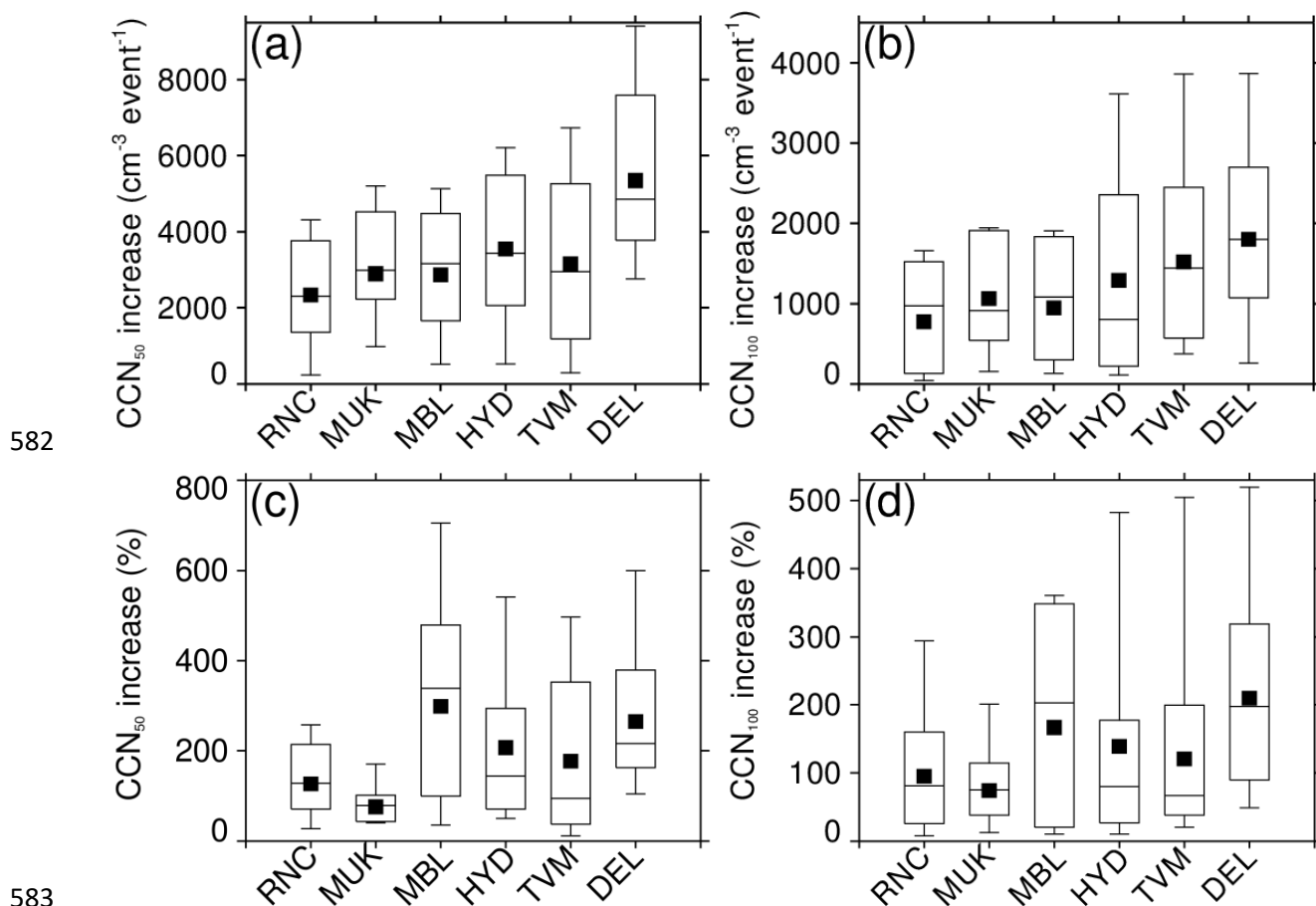
543
 544 **3.2.3 Increase in CCN concentrations during NPF events**

545 To reach climatologically relevant sizes, the newly formed particles must grow by
 546 condensation while avoiding coagulation removal by pre-existing particles because these freshly
 547 formed particles are small and highly diffusive (Vehkamäki and Riipinen, 2012). Based on the

548 observed range of particle growth rates at all the sites (0.2 to 17.3 nm h^{-1}), newly formed particles
549 may take from a few hours to 1-2 days to grow to CCN-active sizes (>50 - 100 nm). Over such time
550 scales, it is observationally challenging to separate CCN originating from NPF from those
551 emanating from the growth of small primary particles and direct emission of CCN-active sized
552 particles. The increase in CCN concentrations during any given NPF event was estimated
553 following the methodology developed by Kerminen et al. (2012), which we modified to remove
554 CCN originating from the growth of small primary particles and direct emission of CCN-active
555 sized particles based on non-event days.

556 Figure 10 shows the box-whisker plot of the absolute increase in CCN concentrations (50
557 and 100 nm) at all the sites. Considering all NPF events at mountain sites, increase in CCN_{50}
558 ranged from 168 cm^{-3} per event to $5.2 \times 10^3 \text{ cm}^{-3}$ per event, with a median value of $2.7 \times 10^3 \text{ cm}^{-3}$
559 per event, whereas the increase in CCN_{100} ranged from $0.02 \times 10^3 \text{ cm}^{-3}$ per event to $1.9 \times 10^3 \text{ cm}^{-3}$
560 per event, with the median value of $1.0 \times 10^3 \text{ cm}^{-3}$ per event. The increase in CCN_{50} and CCN_{100} is
561 about two-fold lower than the free tropospheric site, Chacaltaya (5240 m amsl , Bolivia), for NPF
562 events started in the boundary layer ($5.1 \times 10^3 \text{ cm}^{-3}$ per event and $1.5 \times 10^3 \text{ cm}^{-3}$ per event for 50 and
563 100 nm , respectively) (Rose et al., 2017). The median increase in CCN_{50} and CCN_{100} at RNC
564 ($2.3 \times 10^3 \text{ cm}^{-3}$ per event and $0.9 \times 10^3 \text{ cm}^{-3}$ per event) and MUK ($2.9 \times 10^3 \text{ cm}^{-3}$ per event and 0.9×10^3
565 cm^{-3} per event) are comparable to those reported at Botsalano (1420 m amsl , South Africa);
566 $2.5 \times 10^3 \text{ cm}^{-3}$ per event and $0.8 \times 10^3 \text{ cm}^{-3}$ per event, respectively, but about three-fold higher than
567 those reported at a remote continental site in Finland ($1.0 \times 10^3 \text{ cm}^{-3}$ per event and $0.2 \times 10^3 \text{ cm}^{-3}$ per
568 event for 50 nm and 100 nm , respectively) (Kerminen et al., 2012). Considering all NPF events at
569 the urban sites, CCN_{50} increase ranged from $0.08 \times 10^3 \text{ cm}^{-3}$ per event to $9.4 \times 10^3 \text{ cm}^{-3}$ per event,
570 with a median value of $4.3 \times 10^3 \text{ cm}^{-3}$ per event, whereas CCN_{100} increase ranged from 0.03×10^3
571 cm^{-3} per event to $4.9 \times 10^3 \text{ cm}^{-3}$ per event, with a median value of $1.2 \times 10^3 \text{ cm}^{-3}$ per event. These
572 values are about two-folds lower as compared to values reported at the station of San Pietro
573 Capofiume, in a polluted region of the Po Valley; $7.3 \times 10^3 \text{ cm}^{-3}$ per event and $2.4 \times 10^3 \text{ cm}^{-3}$ per
574 event, respectively for 50 nm and 100 nm (Laaksonen et al., 2005). High background number
575 concentrations of CCN_{50} and CCN_{100} in Delhi resulted in a smaller relative increase of CCN from
576 NPF during post-monsoon and winter seasons when compared to the other sites. In order to
577 comprehensively investigate the atmospheric CCN budget and the contribution of NPF to it,
578 Kerminen et al. (2012) pointed out that the analysis should include not only NPF events but also

579 non-event days. Therefore, the modified methodology applied here following Kerminen et al.
 580 (2012) provides the best representative of the increase in CCN concentrations for an NPF event.
 581



582

583

584 **Figure 10.** Box-whisker plot of absolute increase in CCN concentrations for (a) 50 nm and (b) 100
 585 nm particles and percentage increase in CCN concentrations for (c) 50 nm and (d) 100 nm at all
 586 the sites based on the observed NPF and non-event events. The filled square indicates the mean,
 587 the horizontal line indicates the median, the top and bottom of the box indicate 25th and 75th
 588 percentile values, and the top and bottom whiskers indicate 10th and 90th percentile values. Note
 589 that measurements are from different time periods for each site (refer to Table 1).

590

591 The sites with low pre-existing particle concentrations (hence, low condensation sink
 592 values), high solar radiation, and cooler temperatures at high-altitude (or free tropospheric) (RNC,
 593 MUK, and MBL) should favor NPF with enhanced frequency as compared to near-surface urban
 594 environments (HYD, TVM, and DEL) wherein pre-existing particles concentration are high,

595 leading to faster removal of nucleating vapors. However, NPF in polluted environments occurs
596 more often than expected, with enhanced growth rates (Yu et al., 2017). Guo et al. (2014) also
597 reported that NPF leads to winter-time haze formation in Beijing. Kulmala et al. (2021) recently
598 showed that >65% of the number concentration of haze particles resulted from NPF in Beijing.
599 The observation sites at altitudes higher than 1000 m amsl also favored NPF at the high
600 condensation sinks and linked precursor gases needed to initiate nucleation and early growth
601 (Sellegrì et al., 2019). Therefore, the low condensation sinks are not necessarily required to trigger
602 nucleation and early growth, provided there are high vapor production rates. The high pre-existing
603 particle concentration is also an indication of precursor-laden air. But when the condensation sink
604 gets very high, it inhibits aerosol nucleation. Further, at Hyderabad, about half of the NPF events
605 did not display aerosol nucleation (sub-3nm particle formation) with subsequent growth of these
606 particles to larger sizes (>10 nm), perhaps due to lower organic vapor concentrations (Sebastian et
607 al., 2021a). Rose et al. (2017) also reported a high frequency of NPF occurrence for boundary layer
608 (48%) than free troposphere (39%) conditions at Chacaltaya mountain (5240 m amsl), Bolivia.
609 Thus potential CCN formation was higher for NPF events initiated in the boundary layer (67%)
610 than free troposphere (53%). Sellegrì et al. (2019) reviewed the CCN concentrations from NPF
611 events in the boundary layer and high-altitude locations. They revealed that the CCN production
612 is the highest at San Pietro Capofiume, a polluted region of the Po Valley ($7.3 \times 10^3 \text{ cm}^{-3}$)
613 (Laaksonen et al., 2005) as compared to high-altitude sites (Rose et al., 2017; Kerminen et al.,
614 2012). Our findings are similar to these studies showing the highest increase in CCN
615 concentrations in urban locations (HYD, TVM, and DEL) compared to mountain locations (RNC,
616 MUK, and MBL) in India. It is not possible to track the nucleated particle until it becomes a CCN,
617 and they are always mixed with CCN originating from primary sources. This makes it extremely
618 difficult to estimate CCN arising from a given NPF event. In the light of the above discussion,
619 these results offer some insights into potential CCN concentrations originating from NPF.

620

621 **4 Conclusions**

622 In this study, we used at least one year of asynchronous particle number size distribution
623 measurements from six locations in India, consisting of mountain background sites (Ranichauri
624 and Mukteshwar), mountain rural site (Mahabaleshwar), urban sites (Delhi and Hyderabad), and
625 semi-urban coastal site (Thiruvananthapuram). The results from this study provide some insights

626 into the processes influencing particle number size distributions and CCN concentrations in
627 different environments (mountain and urban) of India.

628 We found that the regional NPF was most common in the pre-monsoon (spring) at all the
629 measurement sites, with an exception at TVM where NPF occurred mostly in the late monsoon
630 season (September), which was linked to the inflow of continental air masses that provided a
631 source of low volatile vapors for nucleation. During pre-monsoon, DEL has the highest frequency
632 of NPF occurrence (63.8%), followed by HYD (28.4%) and MBL (15.9%). NPF was the least
633 common during winter at all the sites, particularly at the mountain-background sites (RNC and
634 MUK) without a single NPF event. The high solar insolation (active photochemistry) and the
635 elevated boundary layer (efficient ventilation leading to low pre-existing particles near the surface)
636 explain the most common occurrence of NPF in the pre-monsoon (spring), but this is not a
637 universal NPF frequency pattern in India and elsewhere globally. We found that the J_{SDS} during
638 NPF events tends to increase with an increasing anthropogenic influence, with an order of
639 magnitude higher in urban areas ($0.12 \text{ cm}^{-3} \text{ s}^{-1}$) than mountain sites ($0.06 \text{ cm}^{-3} \text{ s}^{-1}$). We did not find
640 any systematic pattern in $\text{GR}_{\text{SDS-25nm}}$, with the highest $\text{GR}_{\text{SDS-25nm}}$ at RNC (6.3 nm h^{-1}) and the
641 lowest at TVM (1.1 nm h^{-1}). The observed values of the NPF frequency, J_{SDS} , and $\text{GR}_{\text{SDS-25nm}}$
642 indicate that the regional NPF events can significantly influence the evolution of particles in the
643 atmosphere. We found that NPF modulates the shape of the particle number size distributions
644 significantly, especially at the mountain background sites (RNC and MUK), which are not directly
645 influenced by the local direct emissions of aerosols (traffic and industries). The number size
646 distribution of particles is higher in pre-monsoon at mountain-background sites, whereas it is
647 higher in winter at urban sites, with the exception of HYD. All sites generally show lower
648 concentrations of particles in monsoon due to the increased removal by wet-scavenging. The
649 histograms of size-segregated particle number concentrations show large variability from one site
650 to another, reflecting the varying contribution of different processes to the total aerosol loading.
651 For instance, the Aitken mode particle concentrations were the highest in pre-monsoon at
652 mountain-background sites (RNC and MUK), whereas they were the highest in winter at urban
653 sites (HYD, TVM, and DEL). Amongst the sites, the lowest measured median total particle number
654 concentration was found in MUK ($2.7 \times 10^3 \text{ cm}^{-3}$) and the highest in DEL ($12.5 \times 10^3 \text{ cm}^{-3}$).

655 We found that the increase in CCN concentrations during an NPF event is higher in urban
656 locations ($4.3 \times 10^3 \text{ cm}^{-3}$ per event and $1.2 \times 10^3 \text{ cm}^{-3}$ per event for 50 nm and 100 nm, respectively)

657 compared to mountain-background sites ($2.7 \times 10^3 \text{ cm}^{-3}$ per event and $1.0 \times 10^3 \text{ cm}^{-3}$ per event for
658 50 nm and 100 nm, respectively). We modified Kerminen and colleagues' approach for removing
659 the potential contribution of primary CCN-active particles to give the best possible estimate for
660 the increase in CCN concentrations during a given NPF event. Such analyses should be
661 supplemented by regional model simulations or high spatial resolution measurements of NPF and
662 CCN concentrations.

663
664 **Code availability**

665 Particle number size distributions data was analyzed in IGOR Pro 8.0. Figure 8 was created in
666 IGOR Pro 8.0, while all other figures were created in IDL 8.0.

667
668 **Data availability**

669 Particles data will be made available upon a reasonable request to the corresponding author.

670
671 **Author contribution:**

672 VPK conceived the idea and designed the research. MS and VPK carried out a comprehensive
673 data analysis. MS carried out CCN estimation analysis and interpretation with critical inputs
674 from JRP, VV, and VPK. MS, SKK, VAK, and SJ performed particle size distribution
675 measurements and analysis. MS and VPK wrote the first draft, and MS edited with critical inputs
676 from all co-authors.

677
678 **Competing interests**

679 The authors declare that they have no conflict of interest.

680
681 **Acknowledgments**

682 VPK was supported by the Department of Science & Technology (DST)-Science Engineering
683 Research Board (SERB) (ECR/2016/001333) and DST-Climate Change Division Program
684 (Aerosol/89/2017). VKS acknowledges the technical support from Sanjay Rawat for maintaining
685 the Climate Monitoring station at Ranichauri. IITM and HACPL are fully funded by the Ministry
686 of Earth Sciences (MoES), Govt. of India. The data collection at Thiruvananthapuram was carried
687 out under the Aerosol Radiative Forcing over India (ARFI) project of the Indian Space Research

688 Organisation-Geosphere Biosphere Program (ISRO-GBP). RKH, VV, EA and APH acknowledge
689 the Academy of Finland Flagship funding (grant no. 337552). RKH and APH also acknowledge
690 the team of TERI, Mukteshwar and V.P. Sharma for technical support. JRP was supported by the
691 US Department of Energy's Atmospheric System Research, an Office of Science, Office of
692 Biological and Environmental Research Program, under grant DE-SC0019000.

693
694 **References**

695 Anil Kumar, V., Hazra, A., Pandithurai, G., Kulkarni, G., Mohan, G. M., Mukherjee, S., Kumar,
696 A. V., Hazra, A., Pandithurai, G., Kulkarni, G., Mohan, G. M., Mukherjee, S., Leena, P. P., Patil,
697 R. D., and Prasad, D. S. V. V. D.: Atmospheric ice nucleating particle measurements and
698 parameterization representative for Indian region, *Atmospheric Research*, 253, 105487,
699 <https://doi.org/10.1016/j.atmosres.2021.105487>, 2021.

700 Babu, S. S., Kompalli, S. K., and Moorthy, K. K.: Aerosol number size distributions over a
701 coastal semi urban location: Seasonal changes and ultrafine particle bursts, *Science of The Total*
702 *Environment*, 563–564, 351-365, <http://dx.doi.org/10.1016/j.scitotenv.2016.03.246>, 2016.

703 Bianchi, F., Junninen, H., Bigi, A., Sinclair, V. A., Dada, L., Hoyle, C. R., Zha, Q., Yao, L.,
704 Ahonen, L. R., Bonasoni, P., Buenrostro Mazon, S., Hutterli, M., Laj, P., Lehtipalo, K.,
705 Kangasluoma, J., Kerminen, V. M., Kontkanen, J., Marinoni, A., Mirme, S., Molteni, U., Petäjä,
706 T., Riva, M., Rose, C., Sellegri, K., Yan, C., Worsnop, D. R., Kulmala, M., Baltensperger, U.,
707 and Dommen, J.: Biogenic particles formed in the Himalaya as an important source of free
708 tropospheric aerosols, *Nature Geoscience*, 14, 4-9, [10.1038/s41561-020-00661-5](https://doi.org/10.1038/s41561-020-00661-5), 2021.

709 Bousiotis, D., Brean, J., Pope, F. D., Dall'Osto, M., Querol, X., Alastuey, A., Perez, N., Petäjä,
710 T., Massling, A., Nøjgaard, J. K., Nordstrøm, C., Kouvarakis, G., Vratolis, S., Eleftheriadis, K.,
711 Niemi, J. V., Portin, H., Wiedensohler, A., Weinhold, K., Merkel, M., Tuch, T., and Harrison, R.
712 M.: The effect of meteorological conditions and atmospheric composition in the occurrence and
713 development of new particle formation (NPF) events in Europe, *Atmos. Chem. Phys.*, 21, 3345-
714 3370, [10.5194/acp-21-3345-2021](https://doi.org/10.5194/acp-21-3345-2021), 2021.

715 Census of India: Provisional population totals: rural-urban distribution Volume 2, Issue 1 of
716 Census of India, 2011, India. India: Office of the Registrar General & Census Commissioner,
717 2011.

718 Dal Maso, M., Kulmala, M., Riipinen, I., Wagner, R., Hussein, T., Aalto, P. P., and Lehtinen, K.
719 E. J.: Formation and growth of fresh atmospheric aerosols: eight years of aerosol size distribution
720 data from SMEAR II, Hyytiälä, Finland, *Boreal Env. Res.*, 10, 323-336, 2005.

721 Dunne, E. M., Gordon, H., Kürten, A., Almeida, J., Duplissy, J., Williamson, C., Ortega, I. K.,
722 Pringle, K. J., Adamov, A., Baltensperger, U., Barmet, P., Benduhn, F., Bianchi, F.,
723 Breitenlechner, M., Clarke, A., Curtius, J., Dommen, J., Donahue, N. M., Ehrhart, S., Flagan, R.
724 C., Franchin, A., Guida, R., Hakala, J., Hansel, A., Heinritzi, M., Jokinen, T., Kangasluoma, J.,
725 Kirkby, J., Kulmala, M., Kupc, A., Lawler, M. J., Lehtipalo, K., Makhmutov, V., Mann, G.,

726 Mathot, S., Merikanto, J., Miettinen, P., Nenes, A., Onnela, A., Rap, A., Reddington, C. L. S.,
727 Riccobono, F., Richards, N. A. D., Rissanen, M. P., Rondo, L., Sarnela, N., Schobesberger, S.,
728 Sengupta, K., Simon, M., Sipilä, M., Smith, J. N., Stozkhov, Y., Tomé, A., Tröstl, J., Wagner, P.
729 E., Wimmer, D., Winkler, P. M., Worsnop, D. R., and Carslaw, K. S.: Global atmospheric
730 particle formation from CERN CLOUD measurements, *Science*, 354, 1119-1124,
731 10.1126/science.aaf2649, 2016.

732 Gani, S., Bhandari, S., Patel, K., Seraj, S., Soni, P., Arub, Z., Habib, G., Hildebrandt Ruiz, L.,
733 and Apte, J. S.: Particle number concentrations and size distribution in a polluted megacity: the
734 Delhi Aerosol Supersite study, *Atmos. Chem. Phys.*, 20, 8533-8549, 10.5194/acp-20-8533-2020,
735 2020.

736 Gordon, H., Kirkby, J., Baltensperger, U., Bianchi, F., Breitenlechner, M., Curtius, J., Dias, A.,
737 Dommen, J., Donahue, N. M., Dunne, E. M., Duplissy, J., Ehrhart, S., Flagan, R. C., Frege, C.,
738 Fuchs, C., Hansel, A., Hoyle, C. R., Kulmala, M., Kürten, A., Lehtipalo, K., Makhmutov, V.,
739 Molteni, U., Rissanen, M. P., Stozkhov, Y., Tröstl, J., Tsagkogeorgas, G., Wagner, R.,
740 Williamson, C., Wimmer, D., Winkler, P. M., Yan, C., and Carslaw, K. S.: Causes and
741 importance of new particle formation in the present-day and preindustrial atmospheres, *Journal*
742 *of Geophysical Research: Atmospheres*, 122, 8739-8760, 10.1002/2017jd026844, 2017.

743 Grimm, H. and Eatough, D. J.: Aerosol Measurement: The Use of Optical Light Scattering for
744 the Determination of Particulate Size Distribution, and Particulate Mass, Including the Semi-
745 Volatile Fraction, *Journal of the Air & Waste Management Association*, 59, 101-107,
746 10.3155/1047-3289.59.1.101, 2009.

747 Guo, S., Hu, M., Zamora, M. L., Peng, J., Shang, D., Zheng, J., Du, Z., Wu, Z., Shao, M., Zeng,
748 L., Molina, M. J., and Zhang, R.: Elucidating severe urban haze formation in China, *Proceedings*
749 *of the National Academy of Sciences*, 111, 17373-17378, 10.1073/pnas.1419604111, 2014.

750 Guo, S., Hu, M., Peng, J., Wu, Z., Zamora, M. L., Shang, D., Du, Z., Zheng, J., Fang, X., Tang,
751 R., Wu, Y., Zeng, L., Shuai, S., Zhang, W., Wang, Y., Ji, Y., Li, Y., Zhang, A. L., Wang, W.,
752 Zhang, F., Zhao, J., Gong, X., Wang, C., Molina, M. J., and Zhang, R.: Remarkable nucleation
753 and growth of ultrafine particles from vehicular exhaust, *Proceedings of the National Academy*
754 *of Sciences*, 117, 3427-3432, 10.1073/pnas.1916366117, 2020.

755 Hooda, R. K., Kivekäs, N., O'Connor, E. J., Collaud Coen, M., Pietikäinen, J.-P., Vakkari, V.,
756 Backman, J., Henriksson, S. V., Asmi, E., Komppula, M., Korhonen, H., Hyvärinen, A.-P., and
757 Lihavainen, H.: Driving Factors of Aerosol Properties Over the Foothills of Central Himalayas
758 Based on 8.5 Years Continuous Measurements, *Journal of Geophysical Research: Atmospheres*,
759 123, 13,421-413,442, 10.1029/2018jd029744, 2018.

760 Hyvärinen, A. P., Lihavainen, H., Komppula, M., Panwar, T. S., Sharma, V. P., Hooda, R. K.,
761 and Viisanen, Y.: Aerosol measurements at the Gual Pahari EUCAARI station: preliminary
762 results from in-situ measurements, *Atmos. Chem. Phys.*, 10, 7241-7252, 10.5194/acp-10-7241-
763 2010, 2010.

764 Hyvärinen, A. P., Lihavainen, H., Komppula, M., Sharma, V. P., Kerminen, V. M., Panwar, T.
765 S., and Viisanen, Y.: Continuous measurements of optical properties of atmospheric aerosols in

766 Mukteshwar, northern India, *Journal of Geophysical Research-Atmospheres*, 114,
767 10.1029/2008JD011489, 2009.

768 IPCC: *Climate Change 2013: The Physical Science Basis. Contribution of Working Group I to*
769 *the Fifth Assessment Report of the Intergovernmental Panel on Climate Change*, Cambridge,
770 United Kingdom and New York, NY, USA, , 1535 pp., 2013.

771 Jose, S., Mishra, A. K., Lodhi, N. K., Sharma, S. K., and Singh, S.: Characteristics of Aerosol
772 Size Distributions and New Particle Formation Events at Delhi: An Urban Location in the Indo-
773 Gangetic Plains, 9, 10.3389/feart.2021.750111, 2021.

774 Kalivitis, N., Kerminen, V. M., Kouvarakis, G., Stavroulas, I., Bougiatioti, A., Nenes, A.,
775 Manninen, H. E., Petäjä, T., Kulmala, M., and Mihalopoulos, N.: Atmospheric new particle
776 formation as a source of CCN in the eastern Mediterranean marine boundary layer, *Atmos.*
777 *Chem. Phys.*, 15, 9203-9215, 10.5194/acp-15-9203-2015, 2015.

778 Kanawade, V. P., Benson, D. R., and Lee, S.-H.: Statistical analysis of 4-year observations of
779 aerosol sizes in a semi-rural continental environment, *Atmospheric Environment*, 59, 30-38,
780 <http://dx.doi.org/10.1016/j.atmosenv.2012.05.047>, 2012.

781 Kanawade, V. P., Sebastian, M., Hooda, R. K., and Hyvärinen, A. P.: Atmospheric new particle
782 formation in India: Current understanding, knowledge gaps and future directions, *Atmospheric*
783 *Environment*, 2021.

784 Kanawade, V. P., Tripathi, S. N., Bhattu, D., and Shamjad, P. M.: Sub-micron particle number
785 size distributions characteristics at an urban location, Kanpur, in the Indo-Gangetic Plain,
786 *Atmospheric Research*, 147–148, 121-132, <http://dx.doi.org/10.1016/j.atmosres.2014.05.010>,
787 2014a.

788 Kanawade, V. P., Tripathi, S. N., Chakraborty, A., and Yu, H.: Chemical Characterization of
789 Sub-micron Aerosols during New Particle Formation in an Urban Atmosphere, *Aerosol and Air*
790 *Quality Research*, 20, 1294-1305, 10.4209/aaqr.2019.04.0196, 2020a.

791 Kanawade, V. P., Srivastava, A. K., Ram, K., Asmi, E., Vakkari, V., Soni, V. K., Varaprasad, V.,
792 and Sarangi, C.: What caused severe air pollution episode of November 2016 in New Delhi?,
793 *Atmospheric Environment*, 222, 117125, <https://doi.org/10.1016/j.atmosenv.2019.117125>,
794 2020b.

795 Kanawade, V. P., Tripathi, S. N., Siingh, D., Gautam, A. S., Srivastava, A. K., Kamra, A. K.,
796 Soni, V. K., and Sethi, V.: Observations of new particle formation at two distinct Indian
797 subcontinental urban locations, *Atmospheric Environment*, 96, 370-379,
798 <http://dx.doi.org/10.1016/j.atmosenv.2014.08.001>, 2014b.

799 Kanawade, V. P., Shika, S., Pöhlker, C., Rose, D., Suman, M. N. S., Gadhavi, H., Kumar, A.,
800 Nagendra, S. M. S., Ravikrishna, R., Yu, H., Sahu, L. K., Jayaraman, A., Andreae, M. O.,
801 Pöschl, U., and Gunthe, S. S.: Infrequent occurrence of new particle formation at a semi-rural

802 location, Gadanki, in tropical Southern India, *Atmospheric Environment*, 94, 264-273,
803 <http://dx.doi.org/10.1016/j.atmosenv.2014.05.046>, 2014c.

804 Kerminen, V.-M., Chen, X., Vakkari, V., Petäjä, T., Kulmala, M., and Bianchi, F.: Atmospheric
805 new particle formation and growth: review of field observations, *Environmental Research*
806 *Letters*, 13, 103003, 10.1088/1748-9326/aadf3c, 2018.

807 Kerminen, V.-M., Paramonov, M., Anttila, T., Riipinen, I., Fountoukis, C., Korhonen, H., Asmi,
808 E., Laakso, L., Lihavainen, H., Swietlicki, E., Svenningsson, B., Asmi, A., Pandis, S. N.,
809 Kulmala, M., and Petäjä, T.: Cloud condensation nuclei production associated with atmospheric
810 nucleation: a synthesis based on existing literature and new results, *Atmos. Chem. Phys.*, 12,
811 12037-12059, 10.5194/acp-12-12037-2012, 2012.

812 Kirkby, J., Curtius, J., Almeida, J., Dunne, E., Duplissy, J., Ehrhart, S., Franchin, A., Gagne, S.,
813 Ickes, L., Kurten, A., Kupc, A., Metzger, A., Riccobono, F., Rondo, L., Schobesberger, S.,
814 Tsagkogeorgas, G., Wimmer, D., Amorim, A., Bianchi, F., Breitenlechner, M., David, A.,
815 Dommen, J., Downard, A., Ehn, M., Flagan, R. C., Haider, S., Hansel, A., Hauser, D., Jud, W.,
816 Junninen, H., Kreissl, F., Kvashin, A., Laaksonen, A., Lehtipalo, K., Lima, J., Lovejoy, E. R.,
817 Makhmutov, V., Mathot, S., Mikkila, J., Minginette, P., Mogo, S., Nieminen, T., Onnela, A.,
818 Pereira, P., Petaja, T., Schnitzhofer, R., Seinfeld, J. H., Sipila, M., Stozhkov, Y., Stratmann, F.,
819 Tome, A., Vanhanen, J., Viisanen, Y., Vrtala, A., Wagner, P. E., Walther, H., Weingartner, E.,
820 Wex, H., Winkler, P. M., Carslaw, K. S., Worsnop, D. R., Baltensperger, U., and Kulmala, M.:
821 Role of sulphuric acid, ammonia and galactic cosmic rays in atmospheric aerosol nucleation,
822 *Nature*, 476, 429-433,
823 [http://www.nature.com/nature/journal/v476/n7361/abs/nature10343.html#supplementary-](http://www.nature.com/nature/journal/v476/n7361/abs/nature10343.html#supplementary-information)
824 [information](http://www.nature.com/nature/journal/v476/n7361/abs/nature10343.html#supplementary-information), 2011.

825 Kompalli, S. K., Babu, S. S., Udayasoorian, C., and Jayabalakrishnan, R. M.: Role of
826 anthropogenic emissions and meteorology on ultrafine particle bursts over a high altitude site in
827 Western Ghats during pre-monsoon, *Journal of Atmospheric and Solar-Terrestrial Physics*, 179,
828 378-388, <https://doi.org/10.1016/j.jastp.2018.09.001>, 2018.

829 Kompalli, S. K., Nair, V. S., Jayachandran, V., Gogoi, M. M., and Babu, S. S.: Particle number
830 size distributions and new particle formation events over the northern Indian Ocean during
831 continental outflow, *Atmospheric Environment*, 238, 117719,
832 <https://doi.org/10.1016/j.atmosenv.2020.117719>, 2020.

833 Komppula, M., Lihavainen, H., Hyvärinen, A. P., Kerminen, V.-M., Panwar, T. S., Sharma, V.
834 P., and Viisanen, Y.: Physical properties of aerosol particles at a Himalayan background site in
835 India, *Journal of Geophysical Research: Atmospheres*, 114, n/a-n/a, 10.1029/2008jd011007,
836 2009.

837 Kuang, C., McMurry, P. H., and McCormick, A. V.: Determination of cloud condensation nuclei
838 production from measured new particle formation events, *Geophysical Research Letters*, 36, n/a-
839 n/a, 10.1029/2009gl037584, 2009.

840 Kulmala, M., Vehkamäki, H., Petäjä, T., Dal Maso, M., Lauri, A., Kerminen, V.-M., Birmili, W.,
841 and McMurry, P. H.: Formation and growth rates of ultrafine atmospheric particles: a review of
842 observations, *Journal of Aerosol Science*, 35, 143-176,
843 <http://dx.doi.org/10.1016/j.jaerosci.2003.10.003>, 2004.

844 Kulmala, M., Riipinen, I., Sipilä, M., Manninen, H. E., Petäjä, T., Junninen, H., Maso, M. D.,
845 Mordas, G., Mirme, A., Vana, M., Hirsikko, A., Laakso, L., Harrison, R. M., Hanson, I., Leung,
846 C., Lehtinen, K. E. J., and Kerminen, V.-M.: Toward Direct Measurement of Atmospheric
847 Nucleation, *Science*, 318, 89-92, 10.1126/science.1144124, 2007.

848 Kulmala, M., Dada, L., Daellenbach, K. R., Yan, C., Stolzenburg, D., Kontkanen, J., Ezhova, E.,
849 Hakala, S., Tuovinen, S., Kokkonen, T. V., Kurppa, M., Cai, R., Zhou, Y., Yin, R., Baalbaki, R.,
850 Chan, T., Chu, B., Deng, C., Fu, Y., Ge, M., He, H., Heikkinen, L., Junninen, H., Liu, Y., Lu, Y.,
851 Nie, W., Rusanen, A., Vakkari, V., Wang, Y., Yang, G., Yao, L., Zheng, J., Kujansuu, J.,
852 Kangasluoma, J., Petäjä, T., Paasonen, P., Järvi, L., Worsnop, D., Ding, A., Liu, Y., Wang, L.,
853 Jiang, J., Bianchi, F., and Kerminen, V.-M.: Is reducing new particle formation a plausible
854 solution to mitigate particulate air pollution in Beijing and other Chinese megacities?, *Faraday*
855 *Discussions*, 226, 334-347, 10.1039/D0FD00078G, 2021.

856 Laaksonen, A., Hamed, A., Joutsensaari, J., Hiltunen, L., Cavalli, F., Junkermann, W., Asmi, A.,
857 Fuzzi, S., and Facchini, M. C.: Cloud condensation nucleus production from nucleation events at
858 a highly polluted region, 32, <https://doi.org/10.1029/2004GL022092>, 2005.

859 Laaksonen, A., Hamed, A., Joutsensaari, J., Hiltunen, L., Cavalli, F., Junkermann, W., Asmi, A.,
860 Fuzzi, S., and Facchini, M. C.: Cloud condensation nucleus production from nucleation events at
861 a highly polluted region, 32, <https://doi.org/10.1029/2004GL022092>, 2005.

862 Laj, P., Bigi, A., Rose, C., Andrews, E., Lund Myhre, C., Collaud Coen, M., Lin, Y.,
863 Wiedensohler, A., Schulz, M., Ogren, J. A., Fiebig, M., Glib, J., Mortier, A., Pandolfi, M.,
864 Petäjä, T., Kim, S. W., Aas, W., Putaud, J. P., Mayol-Bracero, O., Keywood, M., Labrador, L.,
865 Aalto, P., Ahlberg, E., Alados Arboledas, L., Alastuey, A., Andrade, M., Artíñano, B., Ausmeel,
866 S., Arsov, T., Asmi, E., Backman, J., Baltensperger, U., Bastian, S., Bath, O., Beukes, J. P.,
867 Brem, B. T., Bukowiecki, N., Conil, S., Couret, C., Day, D., Dayantolis, W., Degorska, A.,
868 Eleftheriadis, K., Fetfatzis, P., Favez, O., Flentje, H., Gini, M. I., Gregorič, A., Gysel-Beer, M.,
869 Hallar, A. G., Hand, J., Hoffer, A., Hueglin, C., Hooda, R. K., Hyvärinen, A., Kalapov, I.,
870 Kalivitis, N., Kasper-Giebl, A., Kim, J. E., Kouvarakis, G., Kranjc, I., Krejci, R., Kulmala, M.,
871 Labuschagne, C., Lee, H. J., Lihavainen, H., Lin, N. H., Lössch, G., Luoma, K., Marinoni, A.,
872 Martins Dos Santos, S., Meinhardt, F., Merkel, M., Metzger, J. M., Mihalopoulos, N., Nguyen,
873 N. A., Ondracek, J., Pérez, N., Perrone, M. R., Petit, J. E., Picard, D., Pichon, J. M., Pont, V.,
874 Prats, N., Prenni, A., Reisen, F., Romano, S., Sellegri, K., Sharma, S., Schauer, G., Sheridan, P.,
875 Sherman, J. P., Schütze, M., Schwerin, A., Sohmer, R., Sorribas, M., Steinbacher, M., Sun, J.,
876 Titos, G., Toczko, B., Tuch, T., Tulet, P., Tunved, P., Vakkari, V., Velarde, F., Velasquez, P.,
877 Villani, P., Vratolis, S., Wang, S. H., Weinhold, K., Weller, R., Yela, M., Yus-Diez, J., Zdimal,
878 V., Zieger, P., and Zikova, N.: A global analysis of climate-relevant aerosol properties retrieved
879 from the network of Global Atmosphere Watch (GAW) near-surface observatories, *Atmos.*
880 *Meas. Tech.*, 13, 4353-4392, 10.5194/amt-13-4353-2020, 2020.

- 881 Merikanto, J., Spracklen, D. V., Mann, G. W., Pickering, S. J., and Carslaw, K. S.: Impact of
882 nucleation on global CCN, *Atmos. Chem. Phys.*, 9, 8601-8616, 10.5194/acp-9-8601-2009, 2009.
- 883 Moorthy, K. K., Satheesh, S. K., Babu, S. S., and Dutt, C. B. S.: Integrated Campaign for
884 Aerosols, gases and Radiation Budget (ICARB): An overview, *Journal of Earth System Science*,
885 117, 243-262, 10.1007/s12040-008-0029-7, 2008.
- 886 Moorthy, K. K., Sreekanth, V., Prakash Chaubey, J., Gogoi, M. M., Suresh Babu, S., Kumar
887 Kompalli, S., Bagare, S. P., Bhatt, B. C., Gaur, V. K., Prabhu, T. P., and Singh, N. S.: Fine and
888 ultrafine particles at a near-free tropospheric environment over the high-altitude station Hanle in
889 the Trans-Himalaya: New particle formation and size distribution, *Journal of Geophysical
890 Research: Atmospheres*, 116, n/a-n/a, 10.1029/2011jd016343, 2011.
- 891 Nair, V. S., Jayachandran, V. N., Kompalli, S. K., Gogoi, M. M., and Babu, S. S.: Cloud
892 condensation nuclei properties of South Asian outflow over the northern Indian Ocean during
893 winter, *Atmos. Chem. Phys.*, 20, 3135-3149, 10.5194/acp-20-3135-2020, 2020.
- 894 Neitola, K., Asmi, E., Komppula, M., Hyvärinen, A. P., Raatikainen, T., Panwar, T. S., Sharma,
895 V. P., and Lihavainen, H.: New particle formation infrequently observed in Himalayan foothills
896 – why?, *Atmos. Chem. Phys.*, 11, 8447-8458, 10.5194/acp-11-8447-2011, 2011.
- 897 Nieminen, T., Kerminen, V.-M., Petäjä, T., Aalto, P. P., Arshinov, M., Asmi, E., Baltensperger,
898 U., Beddows, D. C. S., Beukes, J. P., Collins, D., Ding, A., Harrison, R. M., Henzing, B., Hooda,
899 R., Hu, M., Hörrak, U., Kivekäs, N., Komsaare, K., Krejci, R., Kristensson, A., Laakso, L.,
900 Laaksonen, A., Leitch, W. R., Lihavainen, H., Mihalopoulos, N., Németh, Z., Nie, W., O'Dowd,
901 C., Salma, I., Sellegri, K., Svenningsson, B., Swietlicki, E., Tunved, P., Ulevicius, V., Vakkari,
902 V., Vana, M., Wiedensohler, A., Wu, Z., Virtanen, A., and Kulmala, M.: Global analysis of
903 continental boundary layer new particle formation based on long-term measurements, *Atmos.
904 Chem. Phys.*, 18, 14737-14756, 10.5194/acp-18-14737-2018, 2018.
- 905 Paasonen, P., Asmi, A., Petäjä, T., Kajos, M. K., Äijälä, M., Junninen, H., Holst, T., Abbatt, J. P.
906 D., Arneth, A., Birmili, W., van der Gon, H. D., Hamed, A., Hoffer, A., Laakso, L., Laaksonen,
907 A., Richard Leitch, W., Plass-Dülmer, C., Pryor, S. C., Räisänen, P., Swietlicki, E.,
908 Wiedensohler, A., Worsnop, D. R., Kerminen, V.-M., and Kulmala, M.: Warming-induced
909 increase in aerosol number concentration likely to moderate climate change, *Nature Geoscience*,
910 6, 438-442, 10.1038/ngeo1800, 2013.
- 911 Pierce, J. R. and Adams, P. J.: Efficiency of cloud condensation nuclei formation from ultrafine
912 particles, *Atmos. Chem. Phys.*, 7, 1367-1379, 10.5194/acp-7-1367-2007, 2007.
- 913 Pierce, J. R., Westervelt, D. M., Atwood, S. A., Barnes, E. A., and Leitch, W. R.: New-particle
914 formation, growth and climate-relevant particle production in Egbert, Canada: analysis from 1
915 year of size-distribution observations, *Atmos. Chem. Phys.*, 14, 8647-8663, 10.5194/acp-14-
916 8647-2014, 2014.
- 917 Pierce, J. R., Leitch, W. R., Liggio, J., Westervelt, D. M., Wainwright, C. D., Abbatt, J. P. D.,
918 Ahlm, L., Al-Basheer, W., Cziczo, D. J., Hayden, K. L., Lee, A. K. Y., Li, S. M., Russell, L. M.,
919 Sjostedt, S. J., Strawbridge, K. B., Travis, M., Vlasenko, A., Wentzell, J. J. B., Wiebe, H. A.,

920 Wong, J. P. S., and Macdonald, A. M.: Nucleation and condensational growth to CCN sizes
921 during a sustained pristine biogenic SOA event in a forested mountain valley, *Atmos. Chem.*
922 *Phys.*, 12, 3147-3163, 10.5194/acp-12-3147-2012, 2012.

923 Pikridas, M., Riipinen, I., Hildebrandt, L., Kostenidou, E., Manninen, H., Mihalopoulos, N.,
924 Kalivitis, N., Burkhardt, J. F., Stohl, A., Kulmala, M., and Pandis, S. N.: New particle formation
925 at a remote site in the eastern Mediterranean, 117, <https://doi.org/10.1029/2012JD017570>,
926 2012.

927 Raatikainen, T., Hyvärinen, A. P., Hatakka, J., Panwar, T. S., Hooda, R. K., Sharma, V. P., and
928 Lihavainen, H.: The effect of boundary layer dynamics on aerosol properties at the Indo-
929 Gangetic plains and at the foothills of the Himalayas, *Atmospheric Environment*, 89, 548-555,
930 <https://doi.org/10.1016/j.atmosenv.2014.02.058>, 2014.

931 Ramanathan, V., Crutzen, P. J., Lelieveld, J., Mitra, A. P., Althausen, D., Anderson, J., Andreae,
932 M. O., Cantrell, W., Cass, G. R., Chung, C. E., Clarke, A. D., Coakley, J. A., Collins, W. D.,
933 Conant, W. C., Dulac, F., Heintzenberg, J., Heymsfield, A. J., Holben, B., Howell, S., Hudson,
934 J., Jayaraman, A., Kiehl, J. T., Krishnamurti, T. N., Lubin, D., McFarquhar, G., Novakov, T.,
935 Ogren, J. A., Podgorny, I. A., Prather, K., Priestley, K., Prospero, J. M., Quinn, P. K., Rajeev, K.,
936 Rasch, P., Rupert, S., Sadourny, R., Satheesh, S. K., Shaw, G. E., Sheridan, P., and Valero, F. P.
937 J.: Indian Ocean Experiment: An integrated analysis of the climate forcing and effects of the
938 great Indo-Asian haze, 106, 28371-28398, <https://doi.org/10.1029/2001JD900133>, 2001.

939 Reddington, C. L., Carslaw, K. S., Spracklen, D. V., Frontoso, M. G., Collins, L., Merikanto, J.,
940 Minikin, A., Hamburger, T., Coe, H., Kulmala, M., Aalto, P., Flentje, H., Plass-Dülmer, C.,
941 Birmili, W., Wiedensohler, A., Wehner, B., Tuch, T., Sonntag, A., O'Dowd, C. D., Jennings, S.
942 G., Dupuy, R., Baltensperger, U., Weingartner, E., Hansson, H. C., Tunved, P., Laj, P., Sellegri,
943 K., Boulon, J., Putaud, J. P., Gruening, C., Swietlicki, E., Roldin, P., Henzing, J. S., Moerman,
944 M., Mihalopoulos, N., Kouvarakis, G., Ždímal, V., Zíková, N., Marinoni, A., Bonasoni, P., and
945 Duchi, R.: Primary versus secondary contributions to particle number concentrations in the
946 European boundary layer, *Atmos. Chem. Phys.*, 11, 12007-12036, 10.5194/acp-11-12007-2011,
947 2011.

948 Rodríguez, S., Van Dingenen, R., Putaud, J.-P., Martins-Dos Santos, S., and Roselli, D.:
949 Nucleation and growth of new particles in the rural atmosphere of Northern Italy—relationship
950 to air quality monitoring, *Atmospheric Environment*, 39, 6734-6746,
951 <https://doi.org/10.1016/j.atmosenv.2005.07.036>, 2005.

952 Rose, C., Sellegri, K., Moreno, I., Velarde, F., Ramonet, M., Weinhold, K., Krejci, R., Andrade,
953 M., Wiedensohler, A., Ginot, P., and Laj, P.: CCN production by new particle formation in the
954 free troposphere, *Atmos. Chem. Phys.*, 17, 1529-1541, 10.5194/acp-17-1529-2017, 2017.

955 Rosenfeld, D., Sherwood, S., Wood, R., and Donner, L.: Climate Effects of Aerosol-Cloud
956 Interactions, *Science*, 343, 379-380, 10.1126/science.1247490, 2014.

957 Sarangi, C., Kanawade, V. P., Tripathi, S. N., Thomas, A., and Ganguly, D.: Aerosol-induced
958 intensification of cooling effect of clouds during Indian summer monsoon, *Nature*
959 *Communications*, 9, 3754, 10.1038/s41467-018-06015-5, 2018.

960 Schobesberger, S., Franchin, A., Bianchi, F., Rondo, L., Duplissy, J., Kürten, A., Ortega, I. K.,
961 Metzger, A., Schnitzhofer, R., Almeida, J., Amorim, A., Dommen, J., Dunne, E. M., Ehn, M.,
962 Gagné, S., Ickes, L., Junninen, H., Hansel, A., Kerminen, V. M., Kirkby, J., Kupc, A.,
963 Laaksonen, A., Lehtipalo, K., Mathot, S., Onnela, A., Petäjä, T., Riccobono, F., Santos, F. D.,
964 Sipilä, M., Tomé, A., Tsagkogeorgas, G., Viisanen, Y., Wagner, P. E., Wimmer, D., Curtius, J.,
965 Donahue, N. M., Baltensperger, U., Kulmala, M., and Worsnop, D. R.: On the composition of
966 ammonia–sulfuric-acid ion clusters during aerosol particle formation, *Atmos. Chem. Phys.*, 15,
967 55-78, 10.5194/acp-15-55-2015, 2015.

968 Sebastian, M., Kanawade, V. P., and Pierce, J. R.: Observation of sub-3nm particles and new
969 particle formation at an urban location in India, *Atmospheric Environment*, 256, 118460,
970 <https://doi.org/10.1016/j.atmosenv.2021.118460>, 2021a.

971 Sebastian, M., Kanawade, V., Soni, V., Asmi, E., Westervelt, D., Vakkari, V., Hyvärinen, A. P.,
972 Pierce, J., and Hooda, R.: New Particle Formation and Growth to Climate-Relevant Aerosols at a
973 Background Remote Site in the Western Himalaya, *Journal of Geophysical Research:*
974 *Atmospheres*, 126, 10.1029/2020JD033267, 2021b.

975 Sellegri, K., Rose, C., Marinoni, A., Lupi, A., Wiedensohler, A., Andrade, M., Bonasoni, P., and
976 Laj, P.: New Particle Formation: A Review of Ground-Based Observations at Mountain
977 Research Stations, *Atmosphere*, 10, 493, 2019.

978 Shika, S., Gadhavi, H., Suman, M. N. S., Ravikrishna, R., and Gunthe, S. S.: Atmospheric
979 aerosol properties at a semi-rural location in southern India: particle size distributions and
980 implications for cloud droplet formation, *SN Applied Sciences*, 2, 1007, 10.1007/s42452-020-
981 2804-2, 2020.

982 Sihto, S. L., Mikkilä, J., Vanhanen, J., Ehn, M., Liao, L., Lehtipalo, K., Aalto, P. P., Duplissy, J.,
983 Petäjä, T., Kerminen, V. M., Boy, M., and Kulmala, M.: Seasonal variation of CCN
984 concentrations and aerosol activation properties in boreal forest, *Atmos. Chem. Phys.*, 11, 13269-
985 13285, 10.5194/acp-11-13269-2011, 2011.

986 Siingh, D., Gautam, A. S., Buchunde, P., and Kamra, A. K.: Classification of the new particle
987 formation events observed at a tropical site, Pune, India, *Atmospheric Environment*, 190, 10-22,
988 <https://doi.org/10.1016/j.atmosenv.2018.07.025>, 2018.

989 Singh, R. P., Dey, S., Tripathi, S. N., Tare, V., and Holben, B.: Variability of aerosol parameters
990 over Kanpur, northern India, 109, <https://doi.org/10.1029/2004JD004966>, 2004.

991 Srivastava, A. K., Soni, V. K., Singh, S., Kanawade, V. P., Singh, N., Tiwari, S., and Attri, S. D.:
992 An early South Asian dust storm during March 2012 and its impacts on Indian Himalayan
993 foothills: A case study, *Science of The Total Environment*, 493, 526-534,
994 <https://doi.org/10.1016/j.scitotenv.2014.06.024>, 2014.

- 995 Tare, V., Tripathi, S. N., Chinnam, N., Srivastava, A. K., Dey, S., Manar, M., Kanawade, V. P.,
996 Agarwal, A., Kishore, S., Lal, R. B., and Sharma, M.: Measurements of atmospheric parameters
997 during Indian Space Research Organization Geosphere Biosphere Program Land Campaign II at
998 a typical location in the Ganga Basin: 2. Chemical properties, 111,
999 <https://doi.org/10.1029/2006JD007279>, 2006.
- 1000 Thomas, A., Sarangi, C., and Kanawade, V. P.: Recent Increase in Winter Hazy Days over
1001 Central India and the Arabian Sea, *Scientific Reports*, 9, 17406, 10.1038/s41598-019-53630-3,
1002 2019.
- 1003 Tripathi, R. M., Khandekar, R. N., and Mishra, U. C.: Size distribution of atmospheric aerosols
1004 in urban sites in India, *Science of The Total Environment*, 77, 237-244,
1005 [https://doi.org/10.1016/0048-9697\(88\)90059-9](https://doi.org/10.1016/0048-9697(88)90059-9), 1988.
- 1006 Tripathi, S. N., Tare, V., Chinnam, N., Srivastava, A. K., Dey, S., Agarwal, A., Kishore, S., Lal,
1007 R. B., Manar, M., Kanawade, V. P., Chauhan, S. S. S., Sharma, M., Reddy, R. R., Gopal, K. R.,
1008 Narasimhulu, K., Reddy, L. S. S., Gupta, S., and Lal, S.: Measurements of atmospheric
1009 parameters during Indian Space Research Organization Geosphere Biosphere Programme Land
1010 Campaign II at a typical location in the Ganga basin: 1. Physical and optical properties, 111,
1011 <https://doi.org/10.1029/2006JD007278>, 2006.
- 1012 Tröstl, J., Herrmann, E., Frege, C., Bianchi, F., Molteni, U., Bukowiecki, N., Hoyle, C. R.,
1013 Steinbacher, M., Weingartner, E., Dommen, J., Gysel, M., and Baltensperger, U.: Contribution of
1014 new particle formation to the total aerosol concentration at the high-altitude site Jungfraujoch
1015 (3580 m asl, Switzerland), *Journal of Geophysical Research: Atmospheres*, 121, 11,692-611,711,
1016 10.1002/2015jd024637, 2016.
- 1017 Vehkamäki, H. and Riipinen, I.: Thermodynamics and kinetics of atmospheric aerosol particle
1018 formation and growth, *Chemical Society Reviews*, 41, 5160-5173, 10.1039/C2CS00002D, 2012.
- 1019 Venzac, H., Sellegri, K., Laj, P., Villani, P., Bonasoni, P., Marinoni, A., Cristofanelli, P.,
1020 Calzolari, F., Fuzzi, S., Decesari, S., Facchini, M.-C., Vuillermoz, E., and Verza, G. P.: High
1021 frequency new particle formation in the Himalayas, *Proceedings of the National Academy of
1022 Sciences*, 105, 15666-15671, 10.1073/pnas.0801355105, 2008.
- 1023 Westervelt, D. M., Pierce, J. R., and Adams, P. J.: Analysis of feedbacks between nucleation
1024 rate, survival probability and cloud condensation nuclei formation, *Atmos. Chem. Phys.*, 14,
1025 5577-5597, 10.5194/acp-14-5577-2014, 2014.
- 1026 Westervelt, D. M., Pierce, J. R., Riipinen, I., Trivitanurak, W., Hamed, A., Kulmala, M.,
1027 Laaksonen, A., Decesari, S., and Adams, P. J.: Formation and growth of nucleated particles into
1028 cloud condensation nuclei: model-measurement comparison, *Atmos. Chem. Phys.*, 13, 7645-
1029 7663, 10.5194/acp-13-7645-2013, 2013.
- 1030 Wiedensohler, A., Cheng, Y. F., Nowak, A., Wehner, B., Achtert, P., Berghof, M., Birmili, W.,
1031 Wu, Z. J., Hu, M., Zhu, T., Takegawa, N., Kita, K., Kondo, Y., Lou, S. R., Hofzumahaus, A.,
1032 Holland, F., Wahner, A., Gunthe, S. S., Rose, D., Su, H., and Pöschl, U.: Rapid aerosol particle

- 1033 growth and increase of cloud condensation nucleus activity by secondary aerosol formation and
 1034 condensation: A case study for regional air pollution in northeastern China, *Journal of*
 1035 *Geophysical Research: Atmospheres*, 114, n/a-n/a, 10.1029/2008jd010884, 2009.
- 1036 Wiedensohler, A., Birmili, W., Nowak, A., Sonntag, A., Weinhold, K., Merkel, M., Wehner, B.,
 1037 Tuch, T., Pfeifer, S., Fiebig, M., Fjåraa, A. M., Asmi, E., Sellegri, K., Depuy, R., Venzac, H.,
 1038 Villani, P., Laj, P., Aalto, P., Ogren, J. A., Swietlicki, E., Williams, P., Roldin, P., Quincey, P.,
 1039 Hüglin, C., Fierz-Schmidhauser, R., Gysel, M., Weingartner, E., Riccobono, F., Santos, S.,
 1040 Grüning, C., Faloon, K., Beddows, D., Harrison, R., Monahan, C., Jennings, S. G., O'Dowd, C.
 1041 D., Marinoni, A., Horn, H. G., Keck, L., Jiang, J., Scheckman, J., McMurry, P. H., Deng, Z.,
 1042 Zhao, C. S., Moerman, M., Henzing, B., de Leeuw, G., Löschau, G., and Bastian, S.: Mobility
 1043 particle size spectrometers: harmonization of technical standards and data structure to facilitate
 1044 high quality long-term observations of atmospheric particle number size distributions, *Atmos.*
 1045 *Meas. Tech.*, 5, 657-685, 10.5194/amt-5-657-2012, 2012.
- 1046 Xiao, M., Hoyle, C. R., Dada, L., Stolzenburg, D., Kürten, A., Wang, M., Lamkaddam, H.,
 1047 Garmash, O., Mentler, B., Molteni, U., Baccarini, A., Simon, M., He, X. C., Lehtipalo, K.,
 1048 Ahonen, L. R., Baalbaki, R., Bauer, P. S., Beck, L., Bell, D., Bianchi, F., Brilke, S., Chen, D.,
 1049 Chiu, R., Dias, A., Duplissy, J., Finkenzeller, H., Gordon, H., Hofbauer, V., Kim, C., Koenig, T.
 1050 K., Lampilahti, J., Lee, C. P., Li, Z., Mai, H., Makhmutov, V., Manninen, H. E., Marten, R.,
 1051 Mathot, S., Mauldin, R. L., Nie, W., Onnela, A., Partoll, E., Petäjä, T., Pfeifer, J., Pospisilova,
 1052 V., Quéléver, L. L. J., Rissanen, M., Schobesberger, S., Schuchmann, S., Stozhkov, Y., Tauber,
 1053 C., Tham, Y. J., Tomé, A., Vazquez-Pufleau, M., Wagner, A. C., Wanger, R., Wang, Y., Weitz,
 1054 L., Wimmer, D., Wu, Y., Yan, C., Ye, P., Ye, Q., Zha, Q., Zhou, X., Amorim, A., Carslaw, K.,
 1055 Curtius, J., Hansel, A., Volkamer, R., Winkler, P. M., Flagan, R. C., Kulmala, M., Worsnop, D.
 1056 R., Kirkby, J., Donahue, N. M., Baltensperger, U., El Haddad, I., and Dommen, J.: The driving
 1057 factors of new particle formation and growth in the polluted boundary layer, *Atmos. Chem.*
 1058 *Phys.*, 2021, 1-28, 10.5194/acp-2020-1323, 2021.
- 1059 Yu, F., Luo, G., Nair, A. A., Schwab, J. J., Sherman, J. P., and Zhang, Y.: Wintertime new
 1060 particle formation and its contribution to cloud condensation nuclei in the Northeastern United
 1061 States, *Atmos. Chem. Phys.*, 20, 2591-2601, 10.5194/acp-20-2591-2020, 2020.
- 1062 Yu, H., Ren, L., and Kanawade, V. P.: New Particle Formation and Growth Mechanisms in
 1063 Highly Polluted Environments, *Current Pollution Reports*, 3, 245-253, 10.1007/s40726-017-
 1064 0067-3, 2017.
- 1065 Zhang, R., Khalizov, A., Wang, L., Hu, M., and Xu, W.: Nucleation and Growth of
 1066 Nanoparticles in the Atmosphere, *Chemical Reviews*, 112, 1957-2011, 10.1021/cr2001756,
 1067 2012.
- 1068